Magee Womens Research Institute and Foundation

Annual Progress Report: 2008 Formula Grant

Reporting Period

July 1, 2009 – December 31, 2009

Formula Grant Overview

The Magee-Womens Research Institute and Foundation received $1,194,952 in formula funds for the grant award period January 1, 2009 through December 31, 2009. Accomplishments for the reporting period are described below.

Research Project 1: Project Title and Purpose

Roles of the Nuclear Receptor Cofactor LCOR in Placental Development and Gene Expression - The nuclear receptor PPARγ (Peroxisome Proliferator-Activated Receptor γ) is a transcription factor essential for placental development, and its deficiency results in early embryonic lethality due to placental failure. One of the key target genes of PPARγ in the placenta is *Muc1*. Our analyses of the transcriptional regulation of *Muc1* by PPARγ identified the novel cofactor LCoR (Lignad-dependent nuclear receptor Co-Repressor) as a strong and specific co-activator of *Muc1* transcription by PPARγ. Coupled with the observation that LCoR expression is enriched in the placenta, these findings underlie the hypothesis that LCoR is a key PPARγ-associated co-activator during placental development. This project will test this hypothesis by phenotypic and gene expression analyses of LCoR-deficient embryos in vivo and by biochemical dissection of the LCoR activity in vitro.

Duration of Project

1/1/2009 - 12/31/2009

Project Overview

This project addresses molecular mechanisms of placental development and gene expression. It focuses on the physiological functions and structure-function relationships of the novel transcriptional cofactor LCoR (Ligand-dependent nuclear receptor Co-Repressor) in the placenta. The focus on LCoR derives from our surprising finding that it dramatically and specifically augments the activation of the *Muc1* promoter by the nuclear receptor PPARγ (Proxisome Proliferator-Activated Receptor γ). Our previous work identified PPARγ as an essential regulator of placental development whose deficiency causes lethal defects, attributable to arrested differentiation of placental trophoblasts that hampers vascularization of the placenta. Our subsequent work identified *Muc1* as a robust and specific target gene of PPARγ in the placenta,

and revealed that the regulation of *Muc1* by PPARγ involves complex interactions between several promoter elements, and by extension, several tissue- and target-specific factors. LCoR now appears to be one of these factors. LCoR has no effect on *Muc1* promoter on its own, and its stimulatory effect depends entirely on PPARγ and RXRα. Moreover, LCoR has no effect on other PPARγ-induced promoters, and hence its PPARγ-dependent effect on *Muc1* is highly selective. The abundant expression of LCoR in the placental labyrinth, alongside *Muc1*, enhances the physiological relevance of their observed relationships in vitro. These findings give rise to three interrelated hypotheses: (1) LCoR functions as a key co-activator of PPARγ on the *Muc1* promoter. (2) By extrapolation, LCoR probably co-activates additional (but not all) PPARγ targets in trophoblasts, and probably other, non PPARγ-dependent genes. (3) Via these associations, LCoR is potentially an important regulator of placental development. These hypotheses underlie three specific aims: (1) To determine the effects of endogenous LCoR on *Muc1* expression by knockdown of *Lcor* in trophoblast cultures and in *Lcor*-null placentas in vivo. (2) To use *Lcor*-null mice for determining the functions of LCoR in development and gene expression of the placenta. (3) To understand the basic molecular functions of LCoR and the basis for its target specificity by dissecting protein motifs of LCoR that contribute to *Muc1* activation on the one hand, and *Muc1* promoter elements important for this effect on the other hand. Together, these studies will expand our knowledge of the molecular underpinnings of placental development and physiology.

Principal Investigator

Yaacov Barak, PhD
Visiting Associate Professor
Magee-Womens Research Institute
204 Craft Avenue
Pittsburgh, PA 15213

Other Participating Researchers

Yoel Sadovsky, MD, Tali Shalom-Barak, DVM – employed by Magee-Womens Research Institute

Expected Research Outcomes and Benefits

This project will advance the basic scientific knowledge in the field of placental development, as well as in the general field of gene regulation. As basic research in the field of placenta biology is not extensive, studies of this nature are crucial for enhancing the knowledge in this field in order to provide a conceptual basis for future diagnosis and treatment of diseases of pregnancy and the developing fetus.

Summary of Research Completed

Specific Aim 1: *To determine the effects of endogenous LCoR on Muc1 expression in culture and in vivo.*

During the second six-month period, we collected additional placentas from E9.5 WT and *Lcor*-null embryos in order to validate and extend our core finding from the first period that *Muc1* expression is significantly down-regulated in the absence of LCoR. Overall, three pools of three WT, *Lcor*$^{+/-}$ and *Lcor*-null placentas each were collected and served to extract RNA. This has taken substantially longer than planned due to temporary reproductive problems in our mouse colony, which have been ultimately resolved. RNA from the WT and null pools was reverse transcribed and subjected to quantitative real-time PCR to assess the expression levels of *Lcor*, *Pparg* and *Muc1*. As shown in Fig. 1, *Lcor* levels reflected the corresponding genotypes and, as shown previously, *Pparg* levels were not significantly different between WT and *Lcor*-null placentas. These independent data reconfirmed the reduction in *Muc1* levels in *Lcor*-null placentas, although the difference (72% or 1.4-fold reduction in *Lcor*-null) was less pronounced than the one found in the previous experiment (2-fold).

Specific Aim 2: *To define the effects of LCoR deficiency on placental development and gene expression.*

During this period we further backcrossed the *Lcor*-targeted mouse colony onto two genetic backgrounds – C57BL/6J (B6) and 129sv/ImJ (129). Subsequent crosses of B6•*Lcor*$^{+/-}$ females with 129•*Lcor*$^{+/-}$ males generated quasi-hybrid *Lcor*-null progeny, in which the effects of the mutation are relatively insulated from the effects of a particular genetic background. This strategy helped us to refine the basic developmental analyses of LCoR-deficient mice.

In the first progress report we reported that *Lcor*-null pups die at or around birth. Our current analyses entailed close monitoring of dams and litters on the actual day of birth, and revealed that B6;129-*Lcor*-null embryos survive to parturition. A few are either stillborn or die at birth (~6-8am), but many survive to the afternoon or evening of their first day; none survived by the next morning. As noted in the previous report, surviving *Lcor*-null pups did not have a milk spot (visible milk in the stomach). However, our new observations now indicate that this is not due to death before suckling, but rather due to failure to suckle. This deficit is not necessarily a direct cause of their perinatal death, but likely contributes to it through dehydration and/or failure to thrive. In addition, *Lcor*-null pups were visibly smaller than their WT littermates.

Motivated by the apparent smaller size of *Lcor*-null newborns, we next examined the potential effects of LCoR on placental and embryonic growth by weighing E18.5 WT, *Lcor*$^{+/-}$ and *Lcor*-null embryos and placentas, a day before birth. We confined our assessments to unborn embryos, as the postnatal non-suckling phenotype of the mutants would skew weight data. As shown in Fig. 2A, E18.5 *Lcor*-null embryos were approximately 15% lighter than WT embryos ($p<0.01$), with *Lcor*$^{+/-}$ embryos not significantly different from WT. In contrast, *Lcor*-null placentas were on average 10% heavier than WT placentas ($p<0.05$), suggesting that they may have potential malformations (Fig. 2B); *Lcor*$^{+/-}$ placentas were not significantly different than WT. Histological examinations at E18.5 revealed no obvious anatomical anomaly in *Lcor*-null embryos (data not

shown), but their placentas exhibited abnormal accumulation of glycogen cells in the spongiotrophoblast layer (Fig. 3), providing potential explanation for the basis of their increased weight.

Specific Aim 3: *To dissect the structure-function relationships of LCoR in Muc1 activation*.

In the second grant period we approached this objective by dissecting LCoR-responsive cis elements in the *Muc1* promoter. A modular reporter construct (termed 69-108) that contains the two promoter modules necessary and sufficient for *Muc1* induction by PPARγ recapitulates the responses of the entire *Muc1* promoter to PPARγ, its agonist rosiglitazone (rosi) and LCoR (Fig. 4). When the proximal PPAR response element and its flanking sequences are excised from this construct (69 spliced onto the -45 position of *Muc1*; 69-45), basal expression in the absence of PPARγ goes up, but overall expression in the presence of PPARγ, rosi and LCoR stays roughly the same (Fig. 4). This demonstrates that the missing sequences are important only for basal repression but do not affect the ability of LCoR to activate *Muc1* positively or negatively. Much of the promoter's basal activity and response to PPARγ were abolished when the 108 proximal bp of the *Muc1* promoter were not preceded by the *56U* element, but this fragment mediated a stronger response to LCoR in the presence of PPARγ and rosi compared to the complete promoter. This response was lost upon further deletion that left only the proximal 76 bp of the promoter, although the PPRE was still intact (Fig. 4). These observations suggest that a previously unaccounted for sequence between -108 and -77 of *Muc1*, which is insufficient for a significant response to PPARγ and rosi, contributes significantly to the response to LCoR.

Through a new collaboration with Dr. John White, McGill University, Montreal, we were subsequently informed that LCoR interacts with, and serves as a specific coactivator for the transcription factor KLF6. Importantly, KLF6 binds the tetranucleotide *GGCG*, which appears in the -108 → -77 fragment at the -79 position, as well as at the -37 position and three times in the *56U* fragment. Moreover, KLF6 is enriched in the placenta, and its mutation in mice leads to early embryonic lethality and phenotypic signatures of placental defects, which would be consistent with a transcription factor that co-regulates essential PPARγ target genes. We accordingly amended our original hypothesis as follows: 1. KLF6 is a crucial transcription factor for *Muc1* expression. 2. LCoR activates *Muc1* promoter through interaction with KLF6. 3. PPARγ licenses the promoter for KLF6 action via derepression of the proximal PPRE, not as a direct anchor for LCoR.

In support of these hypotheses Fig. 5 shows that KLF6 indeed induces the *Muc1* promoter in a dramatic fashion, and acts both independently of and additively with LCoR. While KLF6 increases *Muc1* promoter activity in the absence of PPARγ, the extent of activity is only 3-5% of its level in the presence of PPARγ, with or without rosi (Fig. 5). These analyses demonstrate that KLF6 is a potential regulator of *Muc1*, whose effects depend on derepression by PPARγ. These effects were specific to *Muc1* promoter and were not observed with the PPARγ target gene *Ldhb*, on which neither LCoR nor KLF6 augmented the responses to PPARγ and rosi (data not shown).

To examine how specific KLF6 is towards the *Muc1* promoter, we compared its contribution to *Muc1* activation, alone and in combination with PPARγ, rosi and LCoR, to those of four other

GGCG-binding KLF/SP protein family members – KLF4, KLF5, KLF7 and SP1. As shown in Fig. 6, SP1 did not affect *Muc1* activity in any combination, while KLF5 was strongly inhibitory across the board. In contrast, the contributions of KLF4 and KLF7 were comparable to that of KLF6 in the presence of PPARγ, with or without rosi. However, unlike KLF6, neither KLF4 nor KLF7 were able to significantly augment the effect of LCoR+PPARγ+rosi combination on the promoter (Fig. 6). These results suggested that while each of KLF4, 6 or 7 could activate *Muc1* upon derepression by PPARγ, only KLF6 could cooperate with LCoR to achieve additive activation.

Next, to test whether the *GGCG* sequence at -79 is central to the response to KLF6 and/or LCoR, we point-mutated its sequence to *TTCG* (designated as GG → TT) in the context of the LCoR-responsive -108 *Muc1* fragment. We then compared the effects of combinations of PPARγ, rosi, LCoR and KLF6 on the native -108 fragment, a -108 fragment whose PPRE was mutated (-108-Nde), the -108 GG → TT fragment and the -76 fragment. As shown in Fig. 7, the PPRE mutation slightly derepressed basal activity of the -108 fragment, but had no significant effect of the nominal activity in the presence of LCoR and/or KLF6. In contrast, the GG → TT mutation dramatically compromised nominal promoter activity in response to any of the factor combinations without affecting the relative effects of PPARγ, rosi, LCoR and KLF6. This suggested that the sequence surrounding the *GGCG* element is important for the overall activity of the -108 fragment, but is dispensable for its responsiveness to all four variables. Finally, activity of the -76 fragment, which lacks the span between -108 and -77, is even lower than that of -108 GG → TT, and more importantly, this fragment has completely lost its responsiveness to LCoR, but not the other factors. This suggests that another motif inside the -108 → -77 fragment, beyond the *GGCG*, is crucial for the effect of LCoR on the proximal *Muc1* promoter.

FIGURES

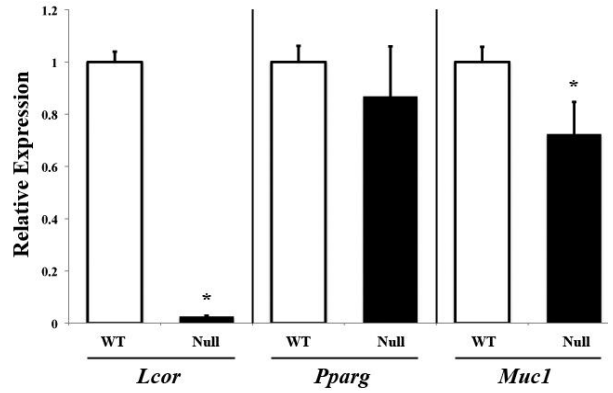

Fig. 1. Effect of LCoR deficiency on placental Muc1 expression (New experiment). Quantitative PCR analysis of relative *Lcor*, *Pparg* and *Muc1* mRNA expression in WT and *Lcor*-null placentas. Asterisks – expression is significantly different than WT placentas ($p<0.05$).

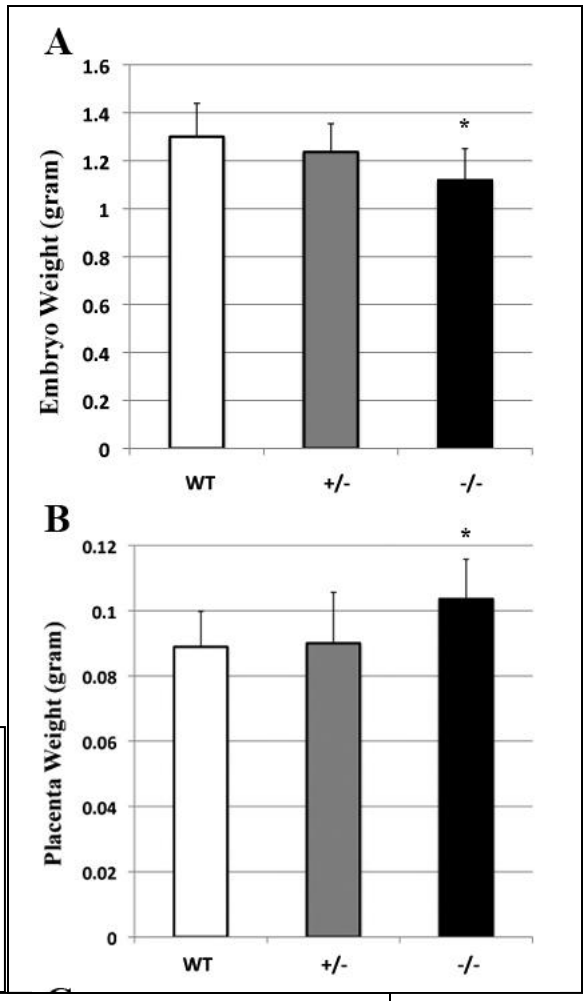

Fig. 2. Weights of E18.5 WT vs Lcor-null embryos and placentas. A. *Embryo weights*. B. placenta weights. Both parameters are significantly different ($P<0.05$) in *Lcor*-null compared to WT specimens. $Lcor^{+/-}$ parameters are not significantly different from WT.

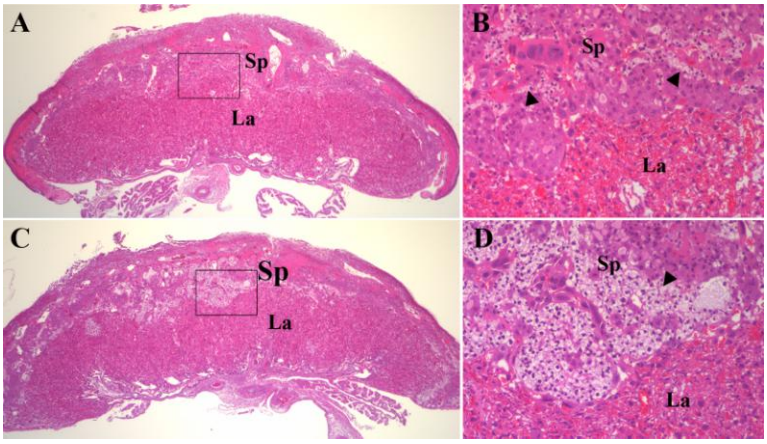

Fig. 3. Histological comparisons of WT and Lcor-null placentas. Hematoxylin and eosin staining of E18.5 WT (A,B) and *Lcor*-null placentas (C,D). Rectangles in A & C mark the insets shown in B & D, respectively. La – labyrinthine layer; Sp – spongiotrophoblast layer. Arrowheads - representative glycogen cells (cells with pale-to-none cytoplasmic staining).

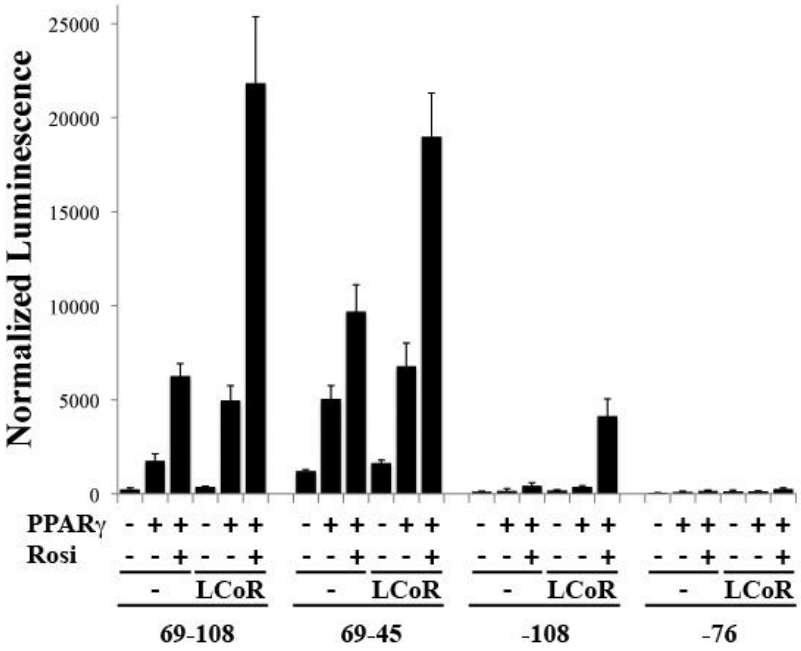

Fig. 4. *LCor-responsive elements in the Muc1 promoter.* CV-1 cells were transfected in triplicates with vectors harboring CMV-*lacZ* and CMV-RXRα (all wells), CMV-PPARγ and CMV-LCoR, as indicated, and the listed *Muc1* promoter-luciferase constructs. Cells were allowed to incubate for 48 hrs either as is or in the presence of 1μM Rosiglitazone (Rosi), as indicated, after which luciferase activity was measured and normalized to β-galactosidase activity of CMV-*lacZ*.

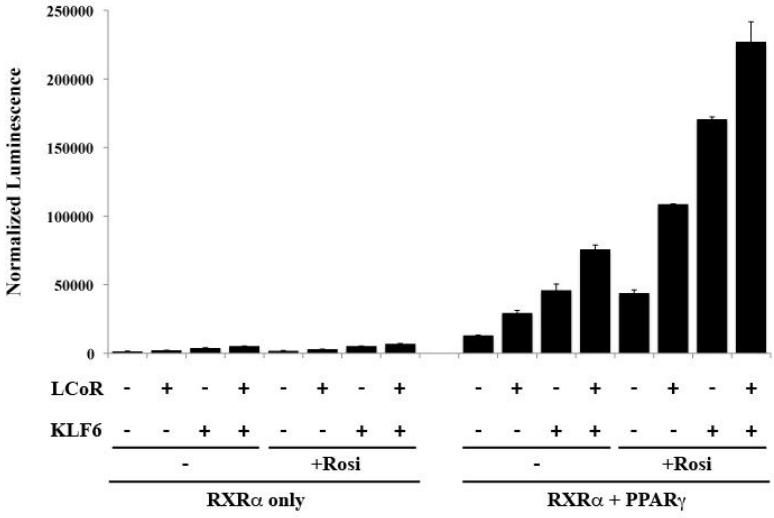

Fig. 5. *KLF6 activates the Muc1 promoter in a PPARg-dependent fashion.* CV-1 cells were transfected in triplicates with a full-length (-715 → +33) *Muc1* promoter-luciferase reporter (all wells), CMV-*lacZ* (all wells), CMV-LCoR and/or CMV-KLF6, as indicated, and either RXRα alone or RXRα + PPARγ, as shown. Cells were incubated for 48 hrs either as is or in the presence of 1μM Rosiglitazone (Rosi), as indicated, after which luciferase activity was measured and normalized to β-galactosidase activity of CMV-*lacZ*.

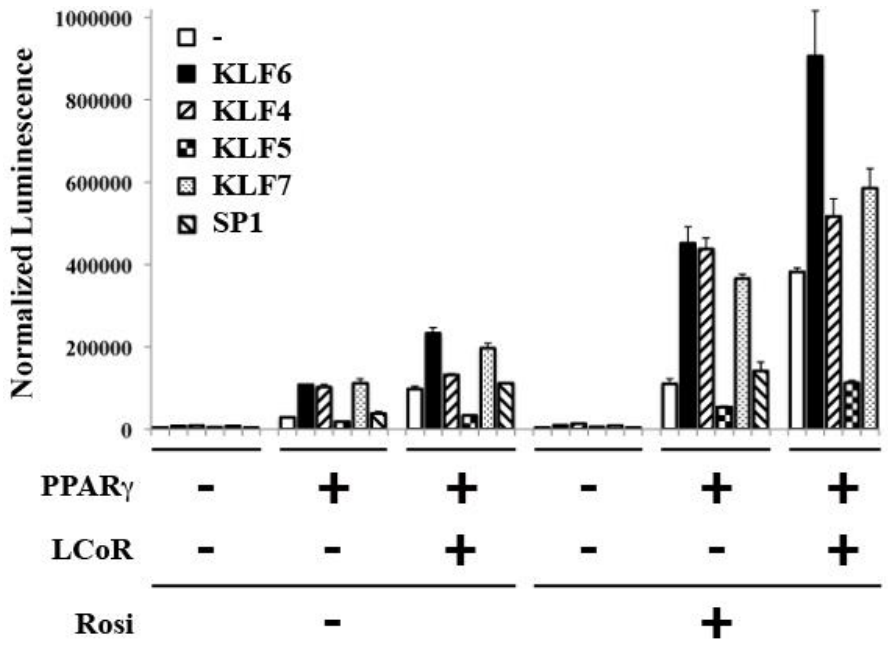

Fig. 6. *Effects of KLF/SP transcription factor family members on Muc1 promoter.* CV-1 cells were transfected in triplicates with full-length *Muc1* promoter, CMV-*lacZ* and CMV-RXRα (all wells), CMV-PPARγ and/or CMV-LCoR, as indicated, and expression vectors encoding KLF/SP proteins, as illustrated. Cells were incubated for 48 hrs either as is or in the presence of 1μM Rosiglitazone (Rosi), as indicated, after which luciferase activity was measured and normalized to β-galactosidase activity of CMV-*lacZ.*

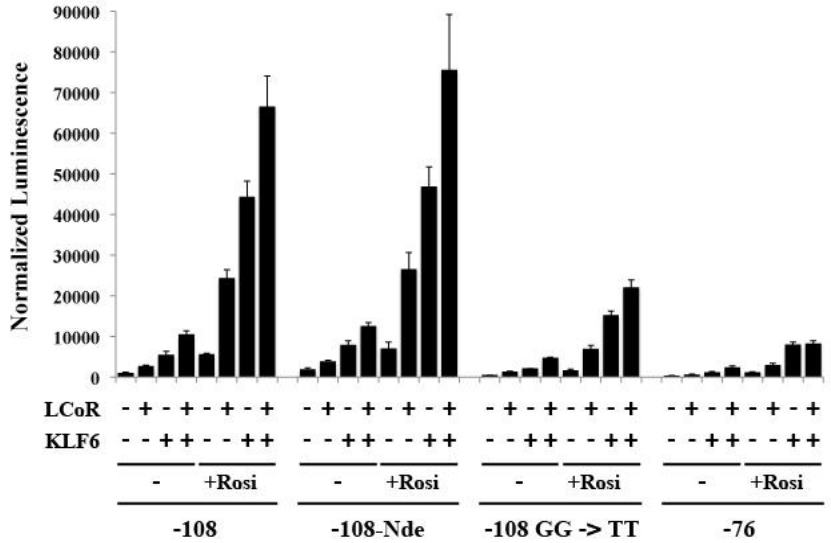

Fig. 7. *The -79 GGCG sequence of Muc1 is important for overall promoter activity, but not essential for LCor or KLF6 responsiveness.* CV-1 cells were transfected in triplicates with CMV-*lacZ*, CMV-RXRα and CMV-PPARγ (all wells), CMV-LCoR and/or CMV-KLF6, as indicated, and the listed *Muc1* promoter-luciferase constructs. Cells were incubated for 48 hrs either as is or in the presence of 1μM Rosiglitazone (Rosi), as indicated, after which luciferase activity was measured and normalized to β-galactosidase activity of CMV-*lacZ.*

Research Project 2: Project Title and Purpose

Establishment of an Animal Model for Respiratory Infection with Influenza during Pregnancy - The purpose of the project is to develop and test a pregnant mouse model for respiratory challenge with influenza virus infection given the disproportionate morbidity and mortality seen among pregnant women during previous influenza pandemics and seasonal epidemics. Development of a pregnant animal model for respiratory challenge will also allow for future investigations to delineate more effectively the susceptibility to infection noted among pregnant women and their immunological response mechanisms. In addition, with the growing threat of bioterrorism and the fact that most of the category A bio-terror agents would be targeted for inhalational spread, development of a pregnant animal model will allow for ongoing research in countermeasures to current and evolving agents of high biological importance in this unique patient population.

Duration of Project

1/1/2009 - 12/31/2009

Project Overview

The broad research objectives are to:

1. Develop a model of collaboration and infrastructure that will allow for ongoing investigation of susceptibility, immunological response and countermeasures to emerging and threatening infectious diseases among pregnant animals.
2. Develop an aerosol delivery challenge model for inhalational influenza among pregnant mice and compare that to non-pregnant mice (controls).
3. Compare whole-body aerosol exposure to nose-only delivery of influenza strain PR/8 (human isolate of seasonal influenza adapted to mice) in pregnant and non-pregnant mice in terms of disease course, clinical signs of morbidity and pathological evaluation at necropsy.
4. Determine the lethal dose (LD_{50}) of a mouse adapted seasonal influenza strain that will kill 50% of the pregnant mouse population and compare to non-pregnant mice. This will be correlated to deposition of influenza virus in the lungs and total body dissemination.

Methods: We will begin by examining aerosol characteristics of influenza at four dilutions in an empty aerosol chamber starting at 10^8/ml and decreasing ten-fold. Four aerosols per dilution (16 aerosols) will use a whole-body exposure box, repeated once for validation. This sequence will be then be repeated with a nose-only tower as a second method of viral challenge. Subsequently we will determine viral concentration in nebulizer and aerosol by Tissue Culture ID50 (TCID50). The next step will be to use two common research strains of adult mice, Balb/c (model for Th-2 adaptive immune response) and BL/6 (model for Th-1 adaptive immune response) to determine the LD_{50} of influenza. Both pregnant and non-pregnant mice will be used and subsequently exposed in a whole-body chamber to aerosolized influenza strain PR/8 at doses expected to bracket the LD_{50} and LD_{99} (~$1x10^3$ and $1x10^5$ pfu, respectively). Mice will be observed for 14 days post-exposure to determine outcome including changes in weight and clinical signs of illness. Mice that become moribund will be promptly euthanized and necropsied; blood and

tissue samples will be taken for analysis. This will then be duplicated in the nose-only fashion. Lastly, both pregnant and non-pregnant mice will be separately aerosol exposed to influenza strain PR8 at a known lethal dose of 100X LD_{50}. At 0, 24, and 48 hours, we will euthanize mice, remove the lungs and fetal compartment (placenta and fetuses) and determine viral load by PCR techniques.

Principal Investigator

Richard H. Beigi, MD, MSc
Assistant Professor of Reproductive Sciences
Magee-Womens Hospital of UPMC
300 Halket Street
Department of OB/GYN/RS
Pittsburgh, PA 15213

Other Participating Researchers

Kelly Stefano-Cole, PhD, Doug Reed, PhD, Amy Hartman, PhD - employed by University of Pittsburgh
Leslie Meyn, MS - employed by Magee-Womens Research Institute

Expected Research Outcomes and Benefits

1. We expect to develop a model for exposing mice to respiratory challenge with influenza. This will allow for comparisons between pregnant and non-pregnant mice which is a unique component of this project. The understanding of pregnant women's increased severity of illness from influenza is not completely understood. In doing these projects, we will have a model to test not only influenza strains of varying potency (including mouse adapted pandemic strains), but will also have a model and working collaboration in place for testing pregnant animals for other respiratory pathogens of high bio-security importance (such as anthrax, smallpox, plague, etc.). This is to our knowledge the only investigations into the pregnancy-specific characteristics of these threatening diseases, and having a rodent animal model will allow us to form a basis for future funded research studies potentially using non-human primates.
2. Eventually, components of what we learn and test will have human relevance in terms of pregnant women's response to such infections but also potentially ways to prevent disease through vaccination and treat such infections in pregnant women. It is important to note that pregnant women are an often forgotten population in terms of research in this area yet are a crucially important sector of the population for many reasons. This research has potentially far reaching implications for societal benefit and protection, as this grant represents the first concrete step in forging this important collaboration between investigators and in developing this animal model on which to build.

Summary of Research Completed

Significant work has continued in the second half of the grant period for this project. The collaboration between the Principal Investigator and the other participating researchers has continued to be fostered and strengthened. This is evidenced by frequent communication, bi-weekly research meetings, and planning and strategic meetings that continue to occur between members of the team. This continues despite different locations within the university and different paradigms of daily work schedules. In committing to these meetings, the collaboration continues to plan for growth and development to allow for testing of new hypotheses and expanding our expertise of aerobiology in pregnant animals. In addition, the work detailed within this report (in addition to the final report) has produced a foundation that supported a recent NIH R21 grant for further study of influenza in pregnancy

A second round of challenge experiments has been performed with both pregnant and non-pregnant mice using the same mouse-adapted A/PR/8/34 (PR8) strain of influenza used in the first round of experiments. The second round of aerosol challenges was done later in gestation (14-16 days vs. 10 days) for 3 reasons:

- Greater ability to verify pregnancy among shipped mice that were supposed to be pregnant
- The time point better approximates 3rd trimester exposure, when human pregnancy appears to be most strongly affected by influenza.
- Closer ability to monitor pregnancy outcomes among recently infected mice (or during time of infection itself).

The goals of the second round of experiments included determination of:

- Detectable differences between pregnant and non-pregnant mice in regards to infectivity and/or severity of illness.
- Repeat validation of the Lethal Dose for 50% of the animals (LD_{50}) that was approximated in the first round of challenges using this particular influenza virus strain and investigating if there is any difference between pregnant and non-pregnant animals in disease course at the same dose.
- The effects of the aerosolized infection using the same mouse-adapted A/PR/8/34 (PR8) strain of influenza on the pregnancy itself (including the effects on the pups from the pregnancy).

The methods for the second round of experiments were as follows:

- 60 mice were obtained for challenges: 30 pregnant and 30 non-pregnant.
- 3 groups of 16 mice (8 pregnant and 8 non-pregnant) were aerosol challenged in the whole-body aerosol exposure using Collison 3-jet nebulizer (AeroMP) using 3 doses of the A/PR/8/34 (PR8) strain of influenza of increasing amounts: 1.4, 22.5, and 27.8 pfu. All pregnant mice were challenged on day 14 of gestation.

- Six pregnant and six non-pregnant mice were sham challenged for control purposes.
- All animals were then monitored for clinical signs & weight change; they were also euthanized when noted to be moribund.

The results of these challenges in terms of weight gain are demonstrated in Figure 1 below. All pregnant mice delivered on day 18 (4 days after challenge). No clear differences were noted in terms of disease effects when comparing pregnant to non-pregnant mice at the same doses. The low dose for both groups showed no difference in terms of disease effects compared to sham controls or compared to each other. However, both middle and high dose groups demonstrate significant effects from influenza aerosol challenge on weight. The effects of the challenges for all pregnant mice together are shown in Figure 2.

From these experiments (and the one round detailed in the first 6 month progress report) the LD_{50} for PR/8 was determined to be 15 pfu, which is approximately ten-fold less than what has been reported for intranasal inoculation with PR/8 in Balb/c mice. There were no differences in LD_{50} noted comparing pregnant vs. non-pregnant.

In terms of the effects of the influenza aerosol challenge on the pregnancy, unexpected findings were noted. Four days after infection with A/PR/8/34, all pregnant mice delivered their pups (day 18 of gestation). It was immediately evident that differences in the number of mice born to each pregnant mouse corresponded with the dose of A/PR/8/34. As shown in Figure 3, mice in the highest dose group delivered an average of 2-3 pups per pregnant mom while the next dose group had an average just under 5 and the lowest dose group and sham group averaged between 5 and 6 pups per pregnant mouse. Some pups had clearly been cannibalized by the mother after birth so it is not clear whether the reduction in litter size was a result of infection or cannibalization by the sick mothers. A similar decline was also seen in the next highest dose group; by day 5 after birth the average litter size was <2 pups per mother. Overall it was noted that influenza challenges had statistically significant effects not only on the size of the litter, but also on the weight of pups at birth, and weight gain of neonatal pups over the first week of life. These noted effects on pups demonstrated a dose-response relationship to the influenza challenge dose.

The results from our first round of experiments combined with the results herein are being used together to move forward with more involved, rigorous, and higher order animal challenges in pregnancy. The funding herein has been instrumental to achieve that endpoint.

Figure 1.

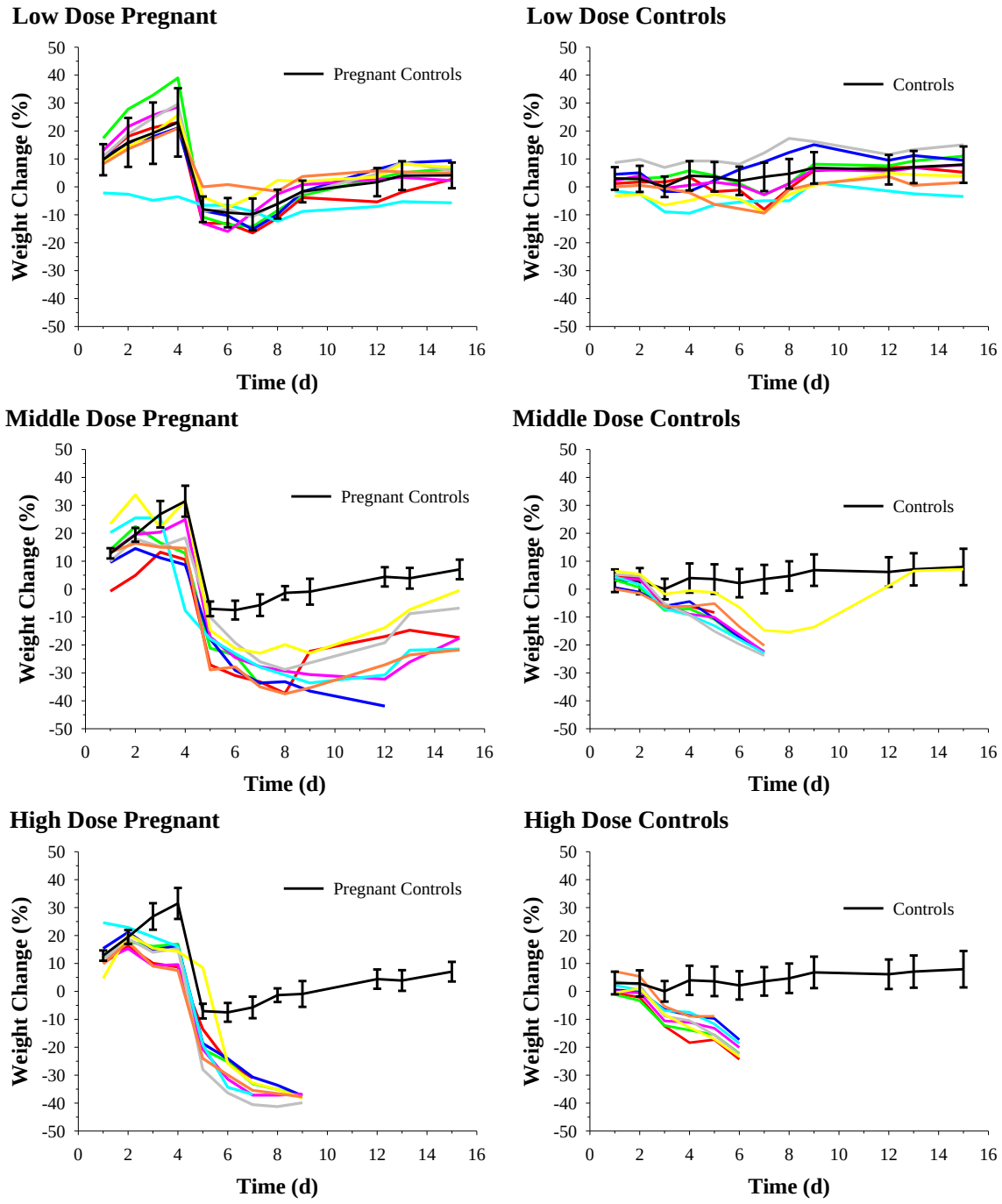
Low Dose Pregnant
Pregnant Controls
Low Dose Controls
Controls
Middle Dose Pregnant
Pregnant Controls
Middle Dose Controls
Controls
High Dose Pregnant
Pregnant Controls
High Dose Controls
Controls
Weight Change (%)
Time (d)

Figure 2. Weight loss in pregnant mice after aerosol exposure to A/PR/8/34.
Graph shows averaged change in weight for each group of pregnant Balb/c mice after exposure to above doses. Weight change in sham infected pregnant controls is shown for comparison; error bars are the standard deviation for the group. Pups were delivered day 4 post-exposure (day 18 of gestation).

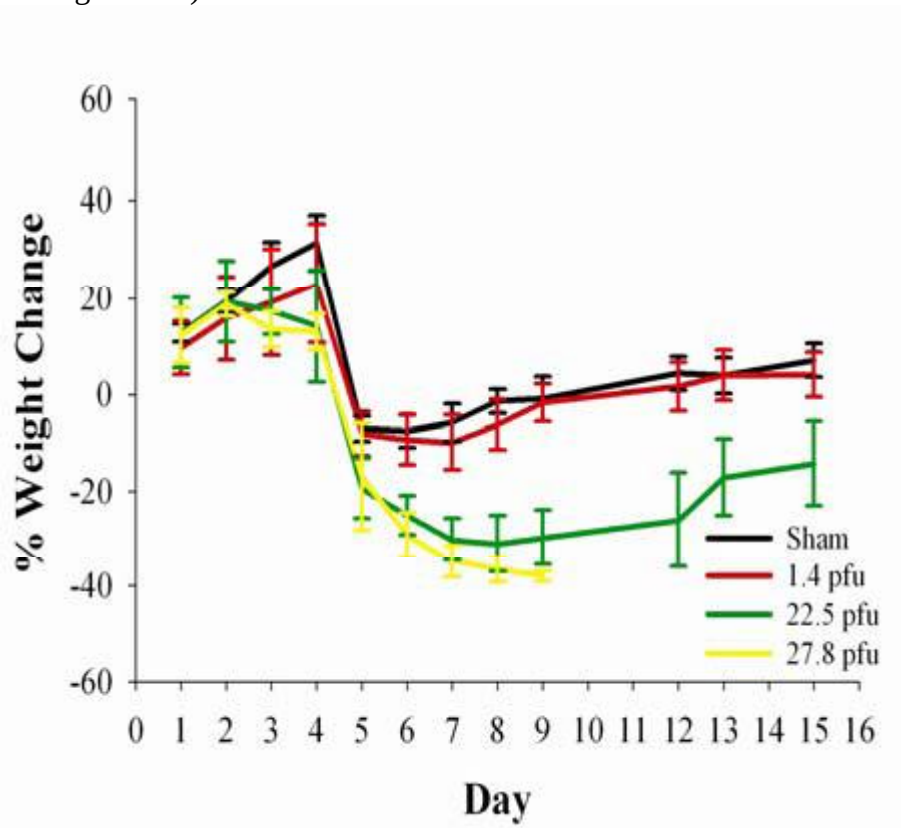

Figure 3.

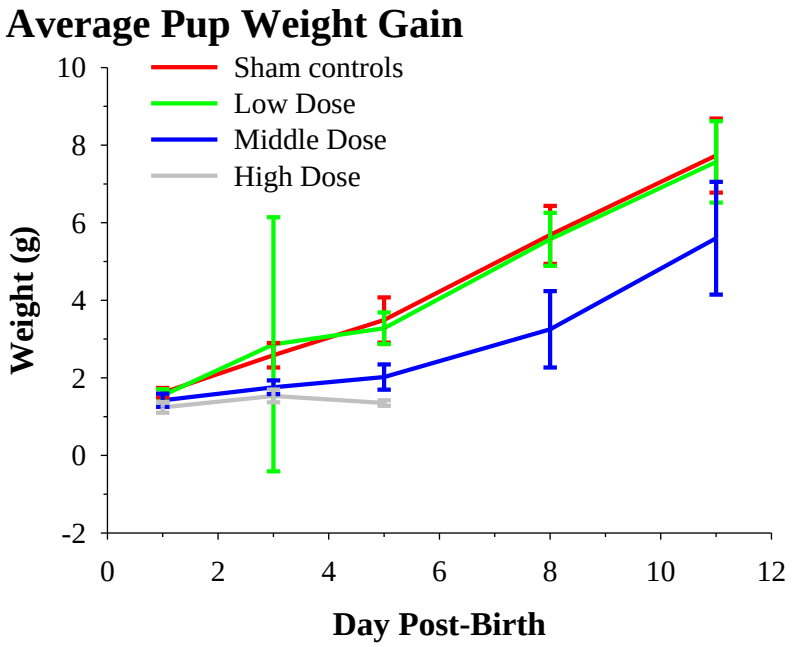
Average Pup Weight Gain
Sham controls
Low Dose
Middle Dose
High Dose
Weight (g)
10
8
6
4
2
0
-2
0
2
4
6
8
10
12
Day Post-Birth

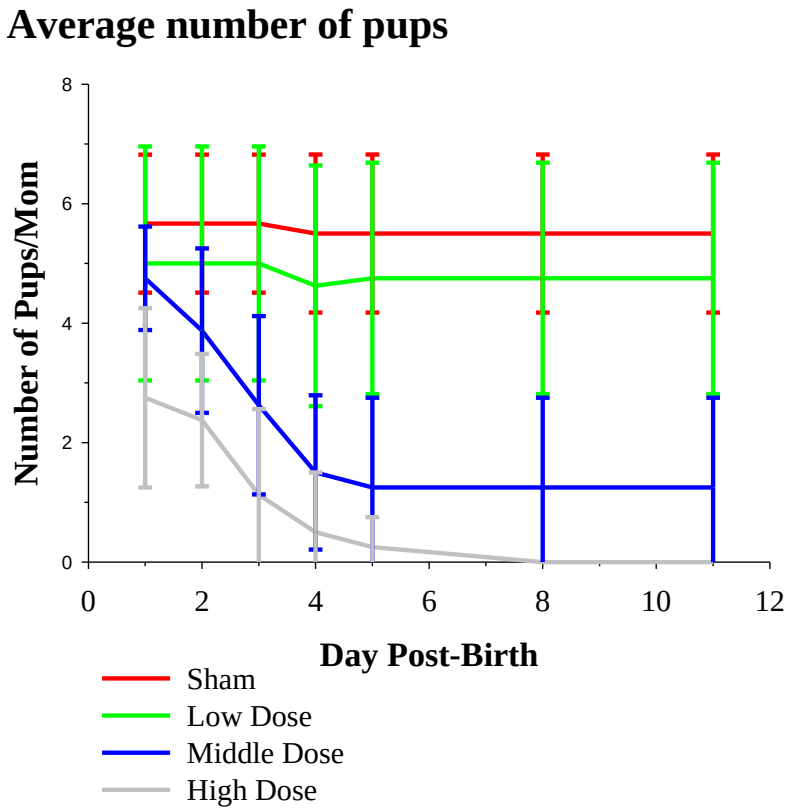
Average number of pups
Number of Pups/Mom
8
6
4
2
0
0
2
4
6
8
10
12
Day Post-Birth
Sham
Low Dose
Middle Dose
High Dose

Research Project 3: Project Title and Purpose

Immune Responses to Herpes Simplex Virus Type 2 and Chlamydia Muridarum in a Murine Model of Co-infection - The number of individuals infected with genital Herpes Simplex Virus Type 2 (HSV-2) has reached epidemic proportions, and considerable evidence suggests that HSV-2 infection of the genital tract facilitates sexual transmission and acquisition of HIV. Recent clinical evidence also suggests that co-infection of the female genital tract with HSV-2 and *Chlamydia trachomatis* results in increased upper genital tract pathology including increased blockage of the Fallopian tubes. However, better elucidation of the immunologic response to HSV-2 is hindered by the lack of an acceptable animal model. We will first establish a female mouse model of genital HSV-2 infection and then use this model to determine the mechanisms used to control vaginal HSV-2 infection and investigate how antecedent HSV-2 infection may modulate the immunologic response to subsequent infections with chlamydia.

Duration of Project

3/9/2009 - 12/31/2009

Project Overview

HSV-2, the primary cause of genital herpes, is a sexually transmitted pathogen that infects the genital tract and produces significant morbidity in humans. As examples, genital herpes infections facilitate sexual transmission and acquisition of HIV, and maternal-fetal transmission of the virus can cause severe and permanent neurological damage to the neonate. A guinea pig model of HSV-2 infection has been developed and extensively studied. A mouse model is also desirable because, in comparison to guinea pigs, a broader array of immunological reagents and knockout strains are available. An adult mouse model of HSV-2 infection has been utilized for studies of primary vaginal infection and for challenge infections after vaginal immunization with attenuated strains of HSV-2. However, they are unsuitable for studies of viral latency and recurrence because the virus typically kills most of the infected mice. To perform studies of HSV-2 latency and recurrence after vaginal infection, a therapeutic intervention that allows the infection to progress from the vagina to the nervous system to establish latent infection but prevents death of the mice is needed. In HSV-2 infected mice, initial viral replication is limited to the vaginal mucosa, which is followed by spread into the central nervous system upon retrograde transport of virions into the sacral ganglia, resulting in a fatal paralysis. In specific aim one, we hypothesize that the adoptive transfer of CD4 cells from acutely infected donor mice to newly infected recipients will limit viral replication, limit viral induced pathology, and improve overall survival. In specific aim two, we hypothesize that regulatory T cells will be the specific CD4 positive donor cells responsible for these effects. In a recent clinical investigation, women co-infected with HSV-2 and *Chlamydia trachomatis* were more likely to be diagnosed with acute endometritis than were women infected with HSV-2 or *C. trachomatis* alone. In specific aim three of this protocol, we will use our model of HSV-2 infection to investigate the effects of antecedent HSV-2 infection on subsequent infection of the genital tract with *Chlamydia muridarum*. We hypothesize the co-infected mice will have significantly greater upper genital tract pathology than mice infected with HSV-2 or *C. muridarum* alone.

Principal Investigator

Thomas L. Cherpes, MD
Assistant Professor
Magee Womens Research Institute
Room A524
204 Craft Avenue
Pittsburgh PA 15213

Other Participating Researchers

None

Expected Research Outcomes and Benefits

There are multiple reasons why it is important to gain a better understanding of the mechanisms used by the host to control HSV-2, the primary cause of genital herpes. Emerging evidence suggests that genital herpes is significantly contributing to the burgeoning HIV pandemic, and each year thousands of infants suffer severe neurologic impairment and death from the acquisition of HSV-2 infection in utero or during passage through the lower genital tract at the time of delivery.

Previous research has demonstrated that both innate (responses present in all individuals at all times which do not increase in intensity with repeated exposure to a pathogen) and adaptive (responses related to interactions between antigen and antigen specific lymphocytes, including the development of immunological memory) host immune responses are important for the control of vaginal HSV-2 infections. Complete elucidation of the host immune responses required for control of vaginal HSV-2 infection is critically needed to better inform the design of effective therapeutic and prophylactic genital herpes vaccines. However, better understanding of these innate and adaptive immune responses is hindered by existing murine models of vaginal HSV-2 infection in which the majority of mice succumb to fatal hindlimb paralysis within 14 days of infection.

This research is expected to produce an experimental model of vaginal HSV-2 infection that allows the virus to progress from the point of primary infection in the vagina and establish a non-lethal, latent (dormant) infection in the central nervous system. The benefits of this model include: better understanding of the immune responses that provide optimal control of primary HSV-2 vaginal infection, more comprehensive delineation of the immune mechanisms used by the host to prevent HSV-2 reactivation from latency, and improved knowledge of the genital tract interactions between HSV-2 and Chlamydia, two of the most common sexually transmitted diseases worldwide.

Summary of Research Completed

HSV-2 infection induces IL-17 mediated inflammatory response associated with tissue damage: Inbred 6-10 week old C57Bl/6 female mice purchased from Jackson Laboratories (Bar Harbor, ME) were used in all of the following studies. To increase susceptibility to infection, all mice were injected subcutaneously with 1.0 mg progesterone 3 days prior to infection. Although the exact mechanism of action is uncertain progesterone increases murine susceptibility to HSV-2 infection - possibly a result of its ability to decrease vaginal epithelial thickness. Mice were anesthetized with a parenteral anesthetic and infected intravaginally with 10 µl of RPMI containing 10^5 PFU of wild-type HSV-2 333. Under the continued influence of anesthetic, mice were placed in ventral recumbency for at least 45 min, a maneuver designed to ensure infectivity of the inoculum. Genital pathology induced by vaginal HSV-2 infection was scored on a 5-point scale as photographically illustrated in Figure 1A. As shown in Figure 2B-C, vaginal HSV-2 infection causes an intense inflammatory infiltrate which is associated with significant tissue damage. Mice that were infected developed progressive genital pathology (all mice were sacrificed when displaying lesions scored as 4 points) and high mortality (Figure 1E-F), associated with viral spread into the CNS that preceded encephalopathy and death (Figure 1G). As a means for continuous monitoring of the inflammatory response to HSV-2, we obtained cells from daily cervicovaginal lavages (CVL) by pipetting 30 µl of phosphate-buffered saline (PBS) in and out of the vagina several times. Obtained cells were stained for flow cytometric analyses. We observed an intense infiltration of neutrophils ($CD11b^+Ly\text{-}6C^+Ly\text{-}6G^+F4/80^-$), inflammatory monocytes ($CD11b^+Ly\text{-}6C^+Ly\text{-}6G^-F4/80^{-/low}$), as well as NK ($CD3^-NK1.1^+MHC\text{-}II^-$) and NKT ($CD3^+NK1.1^+MHC\text{-}II^-$) cells, early in the course of infection (Figure 1H). However, we were unable to detect any substantial lymphocyte populations in these CVL samples. In order to study the lymphocyte infiltrate, we also sacrificed infected mice at day 6 post-infection (dpi 6). We harvested vagina, uterus and regional dorsal root ganglia (DRG) from these mice, and collagenase digested the tissues to obtain single cell suspensions. We were able to observe substantial infiltration of $CD4^+$ and $CD8^+$ T cells in the collected tissues (Figure 1I). We further characterized the infiltrating $CD8^+$ T cell population and determined that a small percentage of cells were capable of recognizing the $gB_{498\text{-}505}/H\text{-}2K^b$ tetramer, indicating that glycoprotein B is not an immunodominant protein during HSV-2 infection (Figure 1J).

Despite intensive prior investigation of vaginal HSV-2 infection in murine models, better understanding of the initial immune response elicited by HSV-2 is needed, and we next investigated inflammatory changes in the vaginal tissue induced by HSV-2 infection. Vaginal tissues from mice vaginally infected with HSV-2 as described above, were obtained daily through dpi 7. Tissues were then mechanically homogenized for total RNA extraction for quantitative real-time PCR analyses and for cytokine/chemokine detection using multiplex technology. As shown in Figure 2A-B, an intense inflammatory response was elicited by vaginal HSV-2 infection. Interestingly, we detected in both CVL and vaginal tissue, a previously unreported production of IL-17 early in the course of the vaginal HSV-2 infection (Figure 2C-D).

In an attempt to identify the cells producing IL-17, we then performed 6 hour *in vivo* brefeldin A (BFA) treatments of mice infected 4 days prior. Tissues were harvested and rendered into single cell suspensions. Using this technique, we identified $CD4^+$ and $CD8^+$ T cells as the main IL-17

producers (Figure 2E), and this data was confirmed by ex vivo stimulation with splenic antigen presenting cells (APCs) loaded with inactivated HSV-2 lysate (Figure 2F). We also observed lower levels IL-17 expression in $CD45^{+}CD3^{-}CD11b^{+}$ cells, and we hypothesize that these are the first cells to produce IL-17 early in the course of infection (Figure 2E).

As IL-17 has been implicated with the immunopathologic damage associated with many viral infections, we next investigated if neutralization of IL-17 using a monoclonal antibody (M210) was capable of preventing tissue damage and mortality. Mice were infected as described above and CVL collected daily for the first 14 dpi were stored at -70° C for posterior detection of replicating virus by plaque assay in order to determine the infection status of each experimental animal (from every recipient mouse we found at least one positive plaque assay on one or more days after infection). As demonstrated in Figures 3A and 3B, inhibition of IL-17 prevented genital pathology and increased survival. Even though we did not test viral replication in these α IL-17 treated animals, it seems likely that the blockade of IL-17 induced an immune response capable of preventing viral invasion of the CNS as viral replication in these tissues has been shown to precede the development of a fatal encephalopathy. Furthermore, αIL-17 treatment was associated with a decrease in the neutrophilic infiltrate (Figure 3C), and increases in the number of inflammatory monocytes and NK cells recruited into the vaginal tissue (Figures 3C and 3D) as shown by analysis of CVL collected 2 dpi. Flow cytometric analysis of the CVL also demonstrated that the naïve vagina contains a high basal number of neutrophils (identified as $CD11b^{+}Ly\text{-}6C^{+}Ly\text{-}6G^{+}F4/80^{-}$ lymphocytes) IL-17 is key element in our defense mechanisms against a variety of pathogens, capable of recruiting neutrophils to limit pathogen replication. However, examination of our model suggests that IL-17 is critical for the elicitation of a response that causes tissue damage but that is also incapable of effectively controlling viral replication and dissemination of the virus to the CNS.

As reported in the first interim progress report, we observed that mice receiving an intravenous transfer of splenocytes from ocularly infected donors were considerable less likely to develop genital tract pathology and more likely to survive vaginal HSV-2 infection (data not shown). As it has been shown that $CD4^{+}$ T cells play a role in disease prevention in mice vaccinated with sub-lethal doses of HSV-2 or with replication deficient virus strains, we next investigated if similar increases in survival of HSV-2 infected mice would be achieved with the transfer of $CD4^{+}$ T cells rather than bulk splenocytes. Donor mice were anesthetized with an injectable anesthetic and corneas were scarified bilaterally prior to infection with 3 µl of RPMI containing $1x10^{3}$ PFU of wild-type HSV-2 333 per eye. Spleens were harvested 7 dpi, and $CD4^{+}$ T cells were selected using the magnetic activated cell sorting (MACS) $CD4^{+}$ T cell Isolation Kit from Miltenyi Biotec. $5x10^{6}$ $CD4^{+}$ splenocytes were transferred intravenously into individual mice (other mice from this same cohort received no transfer of splenocytes). Furthermore, to determine if the beneficial effects on the development of genital pathology produced by transfer of $CD4^{+}$ splenocytes from infected donors was the result of $CD4^{+}$ T cell effector functions mediated by IFN-γ production, a group of mice receiving donor splenocytes from ocularly infected HSV-2 IFN- $\gamma^{-/-}$ mice was also included. All mice were then vaginally infected with $1x10^{5}$ PFU of wild-type HSV-2 333. CVL were obtained as described for detection of replicating virus or analyzed using real-time polymerase chain reaction (rt-PCR) to determine HSV-2 copy number. As demonstrated in Figure 4A, mice that received the transfer of $CD4^{+}$ T cells from ocularly infected donors concomitant with vaginal infection demonstrated decreased genital

pathology and a decreased rate of mortality compared to mice that did not receive transfer of these cells. Moreover, mice receiving IFN-γ $^{-/-}$ donors demonstrated similar decreases in genital pathology and mortality compared to control mice. These results strongly suggest that the mechanism underlying the improved outcomes observed with transfer of $CD4^+$ T cells from ocularly infected donors is not dependent of the release of IFN-γ from transferred splenocytes. Of note, we also explored the possibility that transferred $CD8^+$ T donor cells might produce similar findings to those seen after transfer of $CD4^+$. However, we observed no apparent contributions from $CD8^+$ T cells for suppression of immunopathology or increased survival as was observed after $CD4^+$ T cell transfer (data not shown).

Because IFN-γ production from $CD4^+$ splenocytes was not needed to confer protection against vaginal HSV-2 infection, we next considered the possibility that the adoptive transfer of regulatory T cells (Tregs) could be contributing to the decrease in genital pathology and mortality observed after vaginal infection. Spleens from wildtype donors ocularly infected with HSV-2 were harvested 7 dpi, and splenocytes were selected using the MACS $CD4^+CD25^+$ Regulatory T Cell Isolation Kit. Either $2x10^5$ $CD4^+CD25^+$ or $2x10^5$ $CD4^+CD25^-$ splenocytes were transferred intravenously into progesterone treated mice (control mice from this same cohort received no adoptive transfer of splenocytes). All mice were then vaginally infected with $1x10^5$ PFU of wild-type HSV-2 333, and observed daily for the presence of genital pathology. Mice that received transfer of $CD4^+CD25^+$ splenocytes demonstrated less genital pathology and were more likely to survive infection long-term than controls or mice that received $CD4^+CD25^-$ splenocytes (Figure 4B). Interestingly, transfer of $CD4^+CD25^-$ cells conferred some protection, compared to control mice, against development of genital pathology and death, and it is possible that these findings may have occurred from the inclusion of small numbers of $Foxp3^+$ Tregs in the $CD4^+CD25^-$ transfer population. To test this hypothesis, we next repeated the experiment using $Foxp3^{+GFP}$ mice as donors, to be able to isolate only $Foxp3^+$ cells from splenocytes of infected donors using flow cytometric cell sorting. As shown in Figure 4C, $7.5x10^4$ $CD4^+Foxp3^{+GFP}$ donor cells were capable of preventing tissue damage and mortality, while $7.5x10^4$ $CD4^+Foxp3^-$ cells did not change the course of the infection as compared to controls. Because transfer of $CD4^+CD25^+$ T cells was associated with more favorable outcomes after vaginal HSV-2 infection, we next determined if, compared to untreated controls, this same intervention altered the kinetics of viral clearance from the lower genital tract and spread into CNS. Using the same experimental set-up described immediately above, we compared, using rt-PCR, the HSV-2 burden in CVL and spinal cord specimens between controls and those mice that received $2x10^5$ $CD4^+CD25^+$ splenocytes concomitant with vaginal HSV-2 infection. Surprisingly, as displayed in Figure 4D, despite significant decreases in genital pathology, no detectable effects on viral burden were observed among mice that received the transferred $CD4^+CD25^+$ splenocytes compared to control mice, however, spinal cord invasion by HSV-2 was almost completely prevented. These results indicate that $Foxp3^+$ Tregs from HSV-2 infected donors induces a complex modulation of the response to HSV-2 that prevents tissue damage while enhancing a response capable of controlling invasive viral replication.

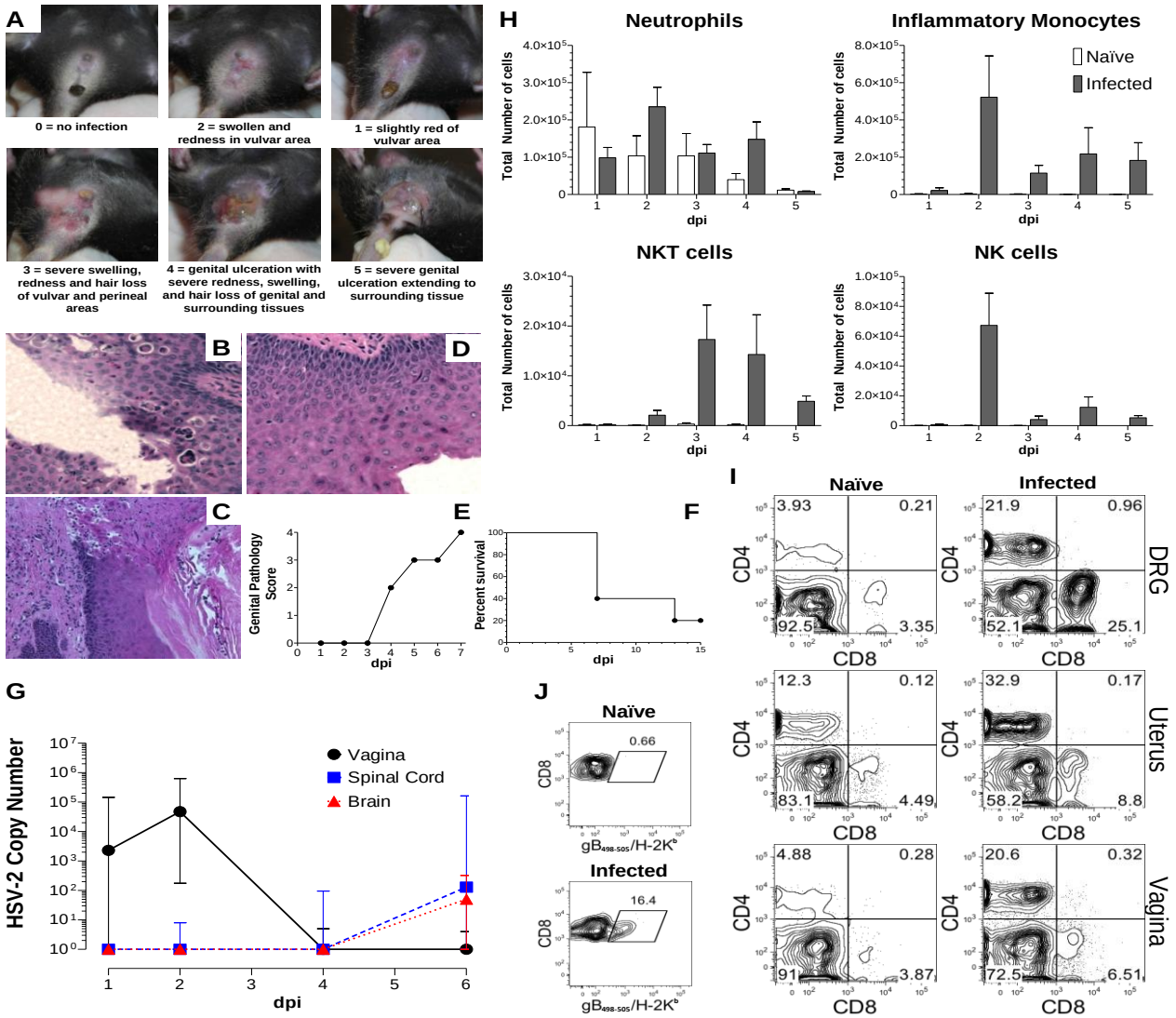

Figure 1. Vaginal HSV-2 infection causes tissue damage associated with recruitment of inflammatory cells. A, Genital tract pathology scoring system. B-D, Vaginal inflammatory infiltrate 7 dpi predominated by PMNs and microabscess formation (B) and disruption of mucosal microarchitecture (C) as compared to control mice (D). (H&E sections viewed with oil immersion). E-F, Mice infected vaginally with HSV-2 develop progressive genital pathology (E) and display high mortality (F) (n=13). G, Lethality and progressive disease is associated with viral invasion of the central nervous system. Data shown is median ±interquartile range (n=31). H, Neutrophils, Inflammatory monocytes, NK and NKT cells are recruited early in the course of infection. Data shown is mean ±SD (n=7 in infected group, n=3 in naïve group). I, $CD4^+$ and $CD8^+$ T cells infiltrate vagina, uterus and DRG late in the course of infection. Dot plots representative from one mouse each representative of experimental groups (n=3). J, A small percentage of CD8+ T cells infiltrating the vagina recognize the $gB_{498\text{-}505}/H\text{-}2K^b$ tetramer (n=3).

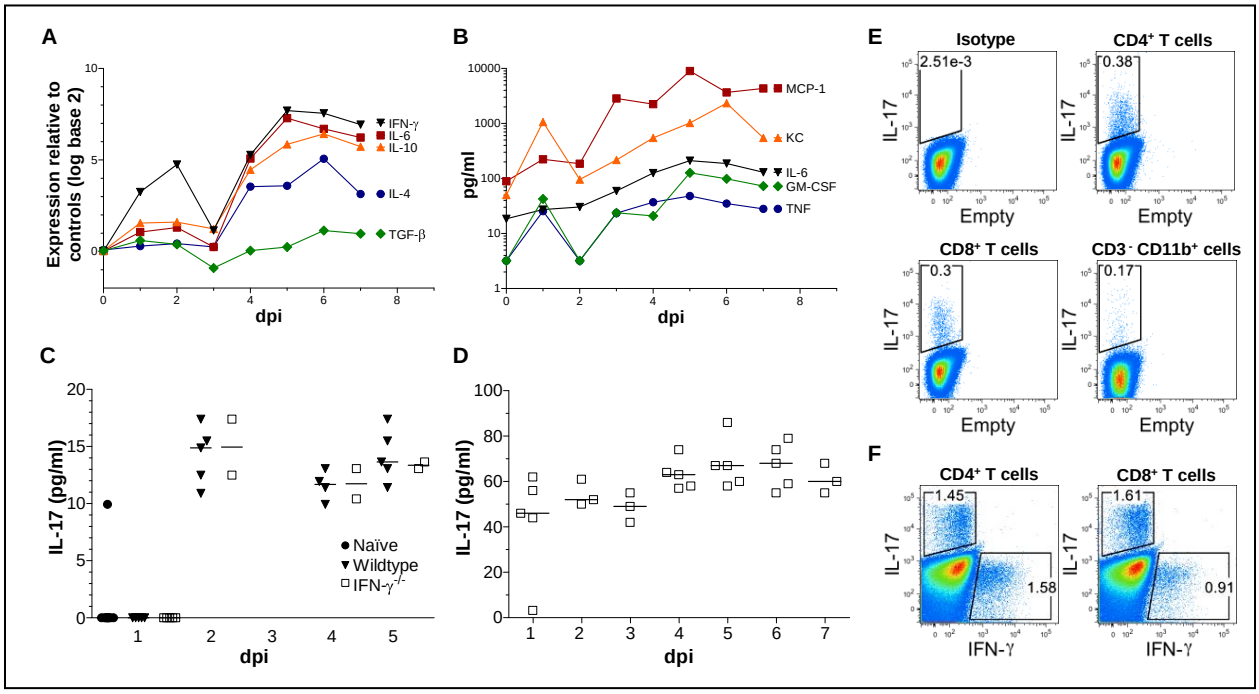

Figure 2. Vaginal HSV-2 infection induces a robust inflammatory response characterized by the production of IL-17. HSV-2 administered vaginally induces high expression of classical inflammatory cytokines as shown by high levels of mRNA expression (**A**) and protein production (**B**). Data shown are means (n=50). One of the molecules induced early in the course of infection is IL-17, which is not normally detected in the CVLs of naïve mice, but it can be readily demonstrated upon HSV-2 infection in CVLs (**C**) and vaginal tissue (**D**). Using BFA *in vivo* treatments we were able to identify some of the cells producing IL-17 on dpi 4. As shown in **E**, CD4+ and CD8+ T cells expressed high levels of IL-17 as shown by ICS, and to a lesser degree $CD45^{+}CD3^{-}CD11b^{+}$ cells (n=5). To confirm the results obtained with BFA treatments, we perform ex vivo stimulation of $CD4^{+}$ and $CD8^{+}$ T cells using splenic antigen presenting cells loaded with inactivated HSV-2 lysate. As shown in **F**, at dpi 6 $CD4^{+}$ and $CD8^{+}$ T cells present in the DLN are capable of producing high levels of IL-17 or IFN-γ, in response to antigen specific stimulation (n=3). Representative pseudocolor plots are shown.

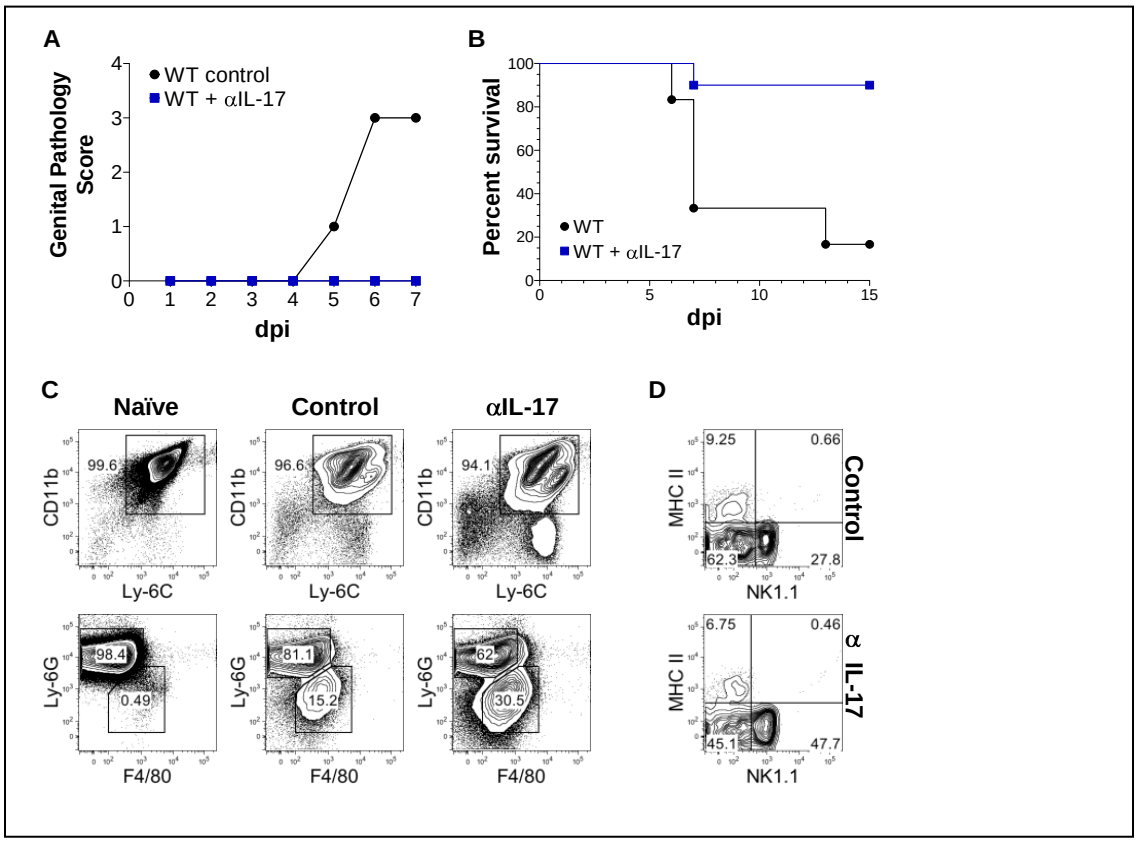

Figure 3. Vaginal HSV-2 infection induces an IL-17 mediated inflammatory response that is associated with tissue damage and cannot prevent viral spread into the CNS. Wildtype mice that received aIL-17 treatment showed less genital pathology (**A**) and increased survival (**B**) after vaginal HSV-2 infection as compared to controls receiving rat IgG**.** One representative experiment of three performed with similar results. Genital pathology scores shown are medians, $p<0.0001$ by two-way ANOVA. Survival curves, $p<0.05$ by Log-rank test. (n=10 in control group, n=10 in αIL-17 treatment group). CVLs were obtained from mice from both groups on dpi 2 for flow cytometric analyses. We observed and increase in inflammatory monocytes and a decrease in the neutrophilic infiltrate (**C**), accompanied by an increase in the number of NK cells present in the examined samples (**D**). Representative contour plots are shown (n=3 in each group).

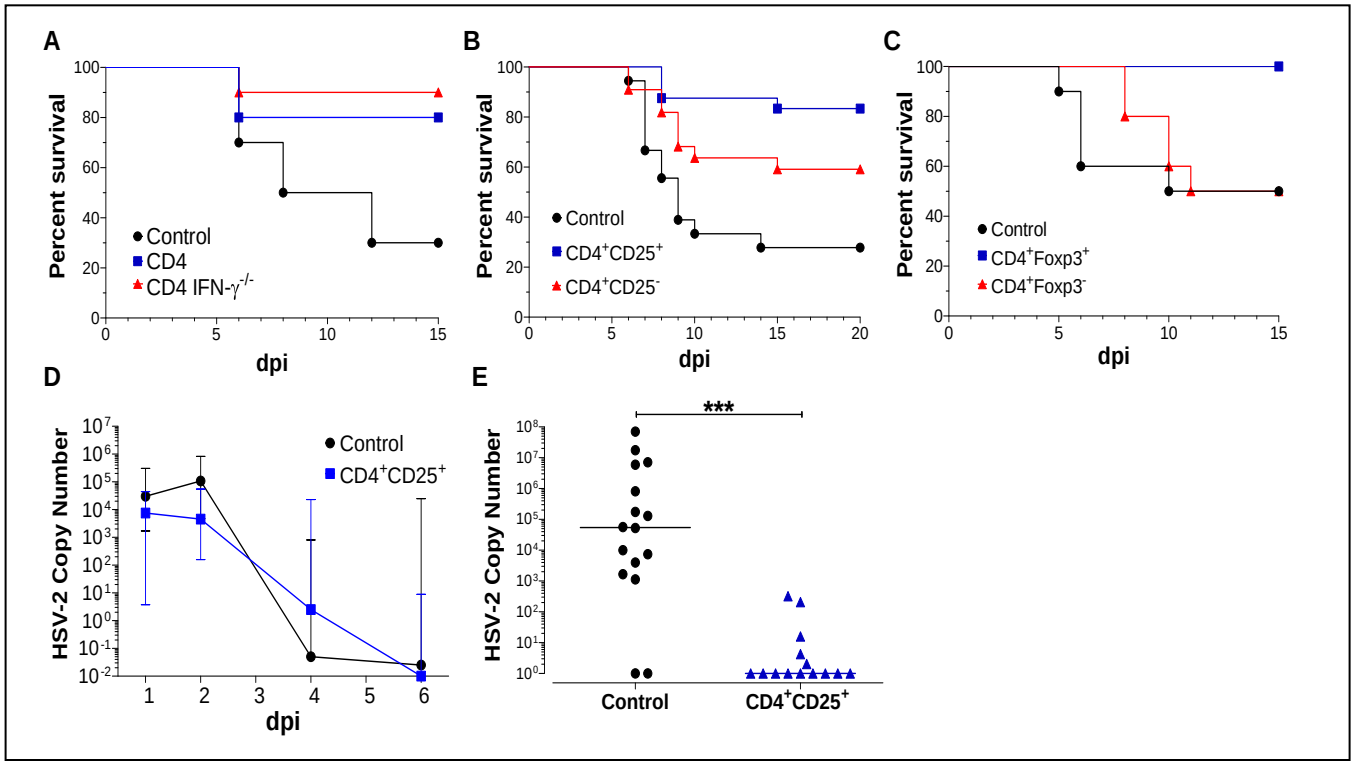

Figure 4. A, Transfer of 5x106 CD4+ wildtype and IFN- γ -/- splenocytes from ocularly infected mice to naïve recipients was associated with reduced pathology and increased survival after vaginal HSV-2 infection. Survival curves, p<0.05 by Log-rank test (n=10 in control group, n=8 in CD4+ group, n=7 in IFN-γ-/- CD4+ group). **B**, Transfer of 2x105 CD4+CD25+ splenocytes from ocularly infected mice to naïve recipients was associated with decreased genital pathology and with increased survival after vaginal HSV-2 infection. Data pooled from 3 experiments; survival curves, p<0.01 by Log-rank test (n=21 in each group). **C**, Transfer of 7.5x104 CD4+Foxp3+GFP splenocytes from ocularly infected mice to naïve recipients was associated with decreased genital pathology and with increased survival after vaginal HSV-2 infection. Survival curves, p<0.05 by Log-rank test (n=7 in control group, n= 6 in Foxp3+ group and n=7 in Foxp3- group). **D**, Similar viral clearance kinetics in the lower genital tract of mice transferred with HSV- induced CD4+CD25+ Tregs. HSV-2 copy numbers shown are median and their interquartile range, p= 0.1520 by two-way ANOVA. (n=14 in control group, n=6 in CD4+CD25+ group). **E**, Transfer of HSV-induced CD4+CD25+ Tregs prevents viral invasion of the spinal cord. HSV-2 copy numbers shown, line indicates mean, p= 0.01 by one-tailed t student test.

Research Project 4: Project Title and Purpose

Integration Study of the Target Genes of PPAR gamma in Human and Mouse Placenta - The Peroxisome Proliferator Activated Receptor gamma (PPAR-gamma) is a transcription factor essential to placental development and function. The main purpose of this project is to identify genes that are affected by PPAR gamma in placenta. The results will lead to better understanding of the mechanism of PPAR gamma in human placenta, and potentially help to prevent or

alleviate many pregnancy complications, such as intrauterine growth restriction (IUGR) and preeclampsia.

Duration of Project

1/1/2009 - 12/31/2009

Project Overview

The Peroxisome Proliferator Activated Receptor gamma (PPAR-gamma) is a transcription factor that plays important roles in many essential processes such as differentiation, metabolism, and inflammation. From the developmental biological point of view, PPAR-gamma is essential to placental development and function.

The main objective of this project to identify potential target genes of PPAR gamma in mouse and human placenta by searching for genes whose expression levels are affected by the change of the expression level or activity of PPAR gamma. The expression level of PPAR gamma could be reduced by knocking out the PPAR gamma gene, or elevated by the induction of PPAR agonists.

In this project, the gene expression data of mouse placenta and mouse and human trophoblast cells for both the treatment (by gene knock-out or adding agonist) and control are generated by two researchers, Drs. Sadovsky and Barak from this institute. Through statistical analysis of the gene expression profiles for the placenta and trophoblast cells (where the PPAR gamma is knocked out or its activity is elevated) and the gene expression profiles for the control, we can generate the list of potential target genes for PPAR gamma in placenta. With the help of gene ontology analysis, we can get further information about which set of main functions and processes these potential target genes are involved.

Principal Investigator

Tianjiao Chu, PhD
Assistant Professor
University of Pittsburgh
204 Craft Ave
B409
Pittsburgh, PA 15213

Other Participating Researchers

Yoel Sadovsky, MD, Yaacov Barak, MD - employed by University of Pittsburgh

Expected Research Outcomes and Benefits

This research project will result in new lists of potential target genes for PPAR gamma in mouse and human placenta. It also will provide the valuable information about how these genes are

regulated by PPAR gamma and specifically how they respond to the change of expression levels and activities in PPAR gamma, as well as the change of the co-activators of PPAR gamma. The results also include the summarization of the main functions of the genes that are up or down regulated by PPAR gamma in human and mouse placenta.

The result will deepen our understanding of the mechanism of PPAR gamma in placenta, shed light on how the gene expression profile of the placenta could be altered through the manipulation of the PPAR gamma, and help the prevention treatment of the diseases caused by disorders of placenta, such as intrauterine growth restriction, preeclampsia, and spontaneous abortion.

Summary of Research Completed

In the second stage of this project, following the study plan, I analyzed the human trophoblast data sets to identify potential direct and indirect targets of PPAR gamma in trophoblast cells, and performed gene ontology analysis to identify the main functions for these genes, as well as the potential direct and indirect target genes in mouse placenta identified in the first 6 months of this study.

A. Identify human genes that are potentially targets of PPAR gamma in placenta

In the first experiment, which will be called the GW 7845/troglitazone experiment, human trophoblast cells collected after 48 hours of differentiation, either treated with one of the two PPAR agonists GW 7845 or troglitazone, or untreated. One sample from each condition was divided into 5 technical replicates, and each technical replicate is hybridized to a set of Affymetrix Human U95 A-E chips. The signal intensity of the probe sets in the Affymetrix arrays were normalized and summarized using the RMA algorithm. The MAANOVA algorithm was applied to test, for each gene, if it was differentially expressed between untreated trophoblast cells and trophoblast cells treated by GW 7845 or troglitazone. The Storey's method was used to calculate the adjusted p values to control the false discovery rate.

With false discovery rate controlled at 10%, 2918 probe sets were found to be differentially expressed either between trophoblast cell control and trophoblast cells treated with GW 7845, or between trophoblast cell control and trophoblast cells treated with troglitazone. For most of these probe sets (2658 out of 2918), if they were up/down regulated in trophoblast cells treated with GW 7845, they were also regulated in the same direction in trophoblast cells treated with troglitazone, and vice versa. This suggested that the two PPAR gamma ligands do have similar effects on the gene expression pattern of trophoblast cells.

Genes significantly regulated in the same direction in both trophoblast cells treated with GW 7845 and trophoblast cells treated with troglizatone (with false discovery rate controlled at 10%) were selected. As shown in the Venn diagram in Figure 1, 55 genes, represented by 83 probe sets, were up regulated significantly in both the trophoblast cells treated with GW 7845 and the trophoblast cells treated with troglitazone, and 94 genes, represented by 120 probe sets, were down regulated significantly in both the trophoblast cells treated with GW 7845 and the trophoblast cells treated with troglitazone.

In the second experiment, which will be called the p38 experiment, human trophoblast samples were collected after 48 hours of differentiation, either treated with PPAR inhibitor p38 or with no treatment. One sample from each condition is hybridized to a set of Affymetrix Human U95 A-E chips. Because there is only a single sample of the trophoblast cells from the treated group and a single sample from the control, and there is no technical replicate, it is impossible to estimate the within-group variance of each gene based on the p38 data set. In other words, using only the data from this second experiment, we could not test if a gene is differentially expressed between the untreated trophoblast cells and the trophoblast cells treated with p38. To solve this problem, I noticed that there are 5 replicates for each trophoblast sample in the previous GW 7845/troglizatone experiment, and normalized and summarized the p38 experiment data together with the data from the GW 7845/troglizatone experiment. Given that the samples in the p38 experiment are similar to the samples in the GW 7845/troglitazone experiment, and the Affymetrix chips from the two experiments were processed together using the RMA algorithm, it is reasonable to assume that the within group variance of the probe sets from the chips in the p38 experiment should be similar to that in the GW 7845/troglitazone experiment

Borrowing the James-Stein shrinkage estimate of the within group variance from the GW 7845/troglitazone experiment, I calculated the F statistics for the probe sets in the p38 experiment. The p values of the F statistics were derived from the empirical distribution of the F statistics, which was also borrowed from the MAANOVA analysis of the GW 7845/troglitazone experiment data. With the false discovery rate controlled at 10%, out of the 55 genes up regulated in the GW 7845/troglitazone experiment, 20 genes, represented by 26 probe sets, were down regulated in trophoblast cells treated with p38. Out of the 94 genes down regulated in the GW 7845/troglitazone experiment, 23 genes, represented by 27 probe sets, were up regulated in trophoblast cells treated with p38.

In the third experiment, which will be called the GW 1929 experiment, human trophoblast samples were collected after 48 hours of differentiation, either treated with GW 1929 or with no treatment. One sample from each condition is hybridized to an Affymetrix Human U95 AV2 chip. Just as in the p38 experiment, in the GW 1929 experiment, there is only a single sample of the trophoblast cells from the treated group and a single sample from the control, and there is no technical replicate. The same procedure used in the analysis of the p38 experiment was also applied to the GW 1929 data, with the estimation of within group variance of each gene, as well as the empirical distribution of the modified F statistics, borrowed from the GW 7845/troglitazone experiment.

Note that the GW 1929 data consists of only Affymetrix U95 AV2 chips, hence not all genes identified in the analysis of p38 experiment were present in the GW 1929 data. In particular, out of the 43 genes selected after the analysis of the p38 experiment, only 20 of them were present in the GW 1929 data. With false discovery rate controlled at 10%, out of these 20 genes, 8 genes were significantly up regulated, and 3 genes significantly down regulated, in the presence of GW 1929.

Combining the analysis of the GW 7845/troglitazone experiment data, p38 experiment data, and GW 1929 experiment data, two lists of genes were identified, as shown in Table 1. The first list

of genes were significantly up regulated in the presence of GW 7845, troglitazone, and GW 1929, but significantly down regulated in the presence of p38. The second list of genes were significantly down regulated in the presence of GW 7845, troglitazone, and GW 1929, but significantly up regulated in the presence of p38. Further experimental data would be needed to establish whether these genes are true targets of PPAR gamma. However, given that PPAR gamma is a transcription factor, based on their expression profile in trophoblast cells treated with various PPAR gamma ligands and inhibitor, it is reasonable to believe that some genes in the first list could be direct target of PPAR gamma in human trophoblast cells, and many genes in the second list could be indirect target of PPAR gamma.

B. Gene ontology analysis of the potential target genes of PPAR gamma in mouse placenta and human trophoblast cells.

In the first stage of this study, two lists of potential direct and indirect targets of PPAR gamma in mouse placenta were identified. Comparing the human homologue of these mouse genes with the list of potential targets of PPAR gamma in human trophoblast cells identified in the second stage of the study, only a single gene, FOLR1, was found to be shared by both the mouse gene list and the human gene list. FOLR1 is likely to be an indirect target of PPAR gamma, as it was always significantly regulated in the opposite direction of PPAR gamma, in both human trophoblast and mouse placenta.

To find out the main functions of the potential direct and indirect target genes identified in mouse placenta and human trophoblast cells, FuncAssociate program was used to perform a gene ontology analysis. For the potential direct targets of PPAR gamma in mouse placenta, with false discovery rate controlled at 5%, 16 attributes were significantly over represented, and 1 under represented, as shown in **Table 2**. In particular, two attributes, peroxisome localization and microtubule-based peroxisome localization, were overrepresented by more than 1000 fold. Many of these overrepresented attributes are closely related to the function of PPAR gamma, suggesting that the list of potential direct targets of PPAR gamma in mouse placenta may contain some true targets.

For the potential indirect targets of PPAR gamma in mouse placenta, only 3 attributes, shown in **Table 2**, were significantly overrepresented with false discovery rate controlled at 10%. For the two lists of potential direct and indirect targets of PPAR gamma in human trophoblast, no attribute was found to be significantly over or under represented. This is mostly likely because of the relatively shorter length of these two gene lists.

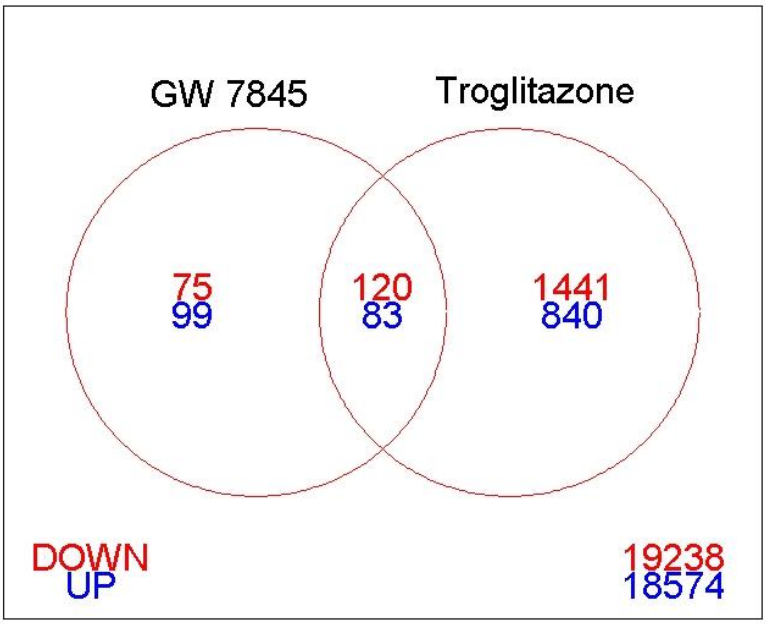

Figure 1. Probes up/down regulated in teh presence of PPAR gamma ligands. 19238 probes down regulated, and 18574 up reguated ,by both ligands. Numbers inside the circles are probe sets significantly up/down regulated, with false discovery rate controlled at 10%.

Potential direct target of PPAR gamma in human trophoblast	Potential indirect target of PPAR gamma in human trophoblast
SLC20A1	LGALS1
CEBPA	FOLR1
ABCG2	CCL2
HMOX1	C1QTNF6
DGKZ	DOCK8
ARL4C	SCD5
CRH	KIAA1432
SLC7A8	ADAMTS1
ANGPTL4	RCN1
TUBB3	HS6ST2
LIMCH1	ITGB6
STARD10	C15orf48
BGN	DDAH1
CDYL	TRPM7
FAM100B	TMTC4
PRDX6	NOVA1
GPR157	
CXorf40A	

Table 1. Potential direct and indirect target genes of PPAR gamma in human trophoblast

Potential Direct Targets in Mouse Placenta		Potential Indirect Targets in Mouse Placenta
Over Represented	Under Represented	Over Represented
peroxisome localization	cellular_component	somatic recombination of immunoglobulin genes during immune response
microtubule-based peroxisome localization		somatic diversification of immunoglobulins during immune response
pyruvate carboxylase activity		isotype switching
L-lactate dehydrogenase activity		
anaerobic glycolysis		
lactate dehydrogenase activity		
biotin binding		
ligase activity, forming carbon-carbon bonds		
gluconeogenesis		
glycolysis		
glucose metabolic process		
oxidoreductase activity, acting on the CH-OH group of donors, NAD or NADP as acceptor		
oxidoreductase activity, acting on CH-OH group of donors		
hexose metabolic process		
monosaccharide metabolic process		
cellular carbohydrate metabolic process		

Table 2. Attributes over represented and under represented in potential target genes of PPAR gamma in mouse placenta

Research Project 5: Project Title and Purpose

Soluble KIT Receptor in the Pathogenesis of Preeclampsia - The purpose of this study is to learn more about what causes the human pregnancy-specific hypertensive disease called preeclampsia. Two factors belonging to a class of proteins known as soluble receptors have been identified in the circulation of women with preeclampsia that appear to damage to the mothers blood vessels and thus contribute to development of the disease. We have discovered that women with preeclampsia are distinguished by abnormally low circulating concentrations of a third soluble receptor *s-kit* (CD117). Evidence exists to suggest that this factor could adversely affect vascular function. We wish to see if *s-kit* increases in the blood early in pregnancy, heralding the development of preeclampsia, consistent with a causal role and/or disease prediction utility, and to study the expression and secretion of this factor by the placenta.

Duration of Project

1/1/2009 - 12/31/2009

Project Overview

It is becoming evident that preeclampsia involves both maternal and feto-placental vascular dysfunction, and that the measurement of (anti)angiogenic factors in maternal blood -- if altered early in pregnancy-- may be useful variables in construction of algorithms for prediction of preeclampsia. Understanding the dysregulation and biological effects of these circulating factors may hasten development of preventative or treatment therapies. During the last three months, we have discovered that women with preeclampsia are distinguished by abnormally low concentrations of the soluble receptor *s-kit* (CD117) in maternal plasma compared to both controls with uncomplicated (normotensive) pregnancies and women with gestational hypertension (without proteinuria). In the non-pregnant setting, low circulating concentrations of *s-kit* are associated with insulin resistance and low circulating concentrations of vascular repair-capable endothelial progenitor cells. Our previous research, funded in part by the PA Department of Health, has shown both insulin resistance and reduced endothelial progenitor cells not only during preeclampsia but also 18 months postpartum after preeclampsia.

The <u>principal hypotheses</u> of this project are 1) that maternal plasma *s-kit* concentrations are reduced early in pregnancy in women who subsequently develop preeclampsia compared to women whose pregnancies remain uncomplicated, 2) that significant differences in circulating *s-kit* remain 18 months postpartum in women with a history of preeclampsia compared to women with a history of uncomplicated pregnancy suggestive of constitutional differences between these groups of women or long-lasting effects of preeclampsia, and 3) that placentas from pregnancies complicated with preeclampsia express lower protein levels of *kit* and SCF (kit-ligand), and secrete lower quantities of *s-kit* and SCF in culture media in an hypoxia-insensitive fashion.

The project will thus begin to investigate the potential importance of the soluble receptor *s-kit* in preeclampsia, potentially the third dysregulated, angiogenic soluble receptor contributing to this pregnancy disorder.

Principal Investigator

Carl A. Hubel, PhD
Assistant Professor
Magee Womens Research Institute and Department OB/GYN & Reproductive Sciences, University Pittsburgh
204 Craft Avenue
Pittsburgh, PA 15213

Other Participating Researchers

Janet M. Catov, PhD, Augustine Rajakumar, PhD - employed by Magee Womens Research Institute and Department OB/GYN & Reproductive Sciences, University Pittsburgh

Expected Research Outcomes and Benefits

The etiology and pathogenesis of the multi-system pregnancy disorder preeclampsia remain poorly understood. Properly functioning vascular endothelial cells--the cells that line the interior of blood vessels-- are vitally important for healthy cardiovascular function and healthy pregnancy. Endothelial dysfunction contributes to development of the signs and symptoms of preeclampsia but the causes of endothelial dysfunction are unclear.

The development of an early pregnancy predictive test for preeclampsia has been called an 'obstetric Holy Grail.' Data are emerging that preeclampsia is an anti-angiogenic state and that the measurement of (anti)angiogenic factors in maternal blood -- if altered early in pregnancy-- could be incorporated into algorithms allowing for an accurate predictive test for preeclampsia, and perhaps provide therapeutic avenues.

During the last several months, we have discovered that women with preeclampsia are distinguished by abnormally low concentrations of the soluble (circulating) receptor *s-kit* (CD117) in maternal plasma compared to both controls with uncomplicated (normotensive) pregnancies or women with just gestational hypertension without other signs of preeclampsia, with little overlap of values. Therefore, we wish to explore the potential role of *s-kit* in the development of preeclampsia. If the hypotheses of this pilot project are supported, it will springboard an NIH proposal to conduct detailed, mechanistic studies on the relationship between the soluble and membrane-bound versions of the *kit* receptor, and their relationship to endothelial progenitor cell function and vascular function during pregnancy in the human and in mouse and cell culture models of preeclampsia.

Although this is not a clinical trial or expected to have immediate 'bench to bedside' translation of research findings to patient care, we expect that this project will significantly advance our understanding of the pathogenesis of preeclampsia. This biomedical research project features collaboration, and is intended for new discovery, leveraging new grants, and potential for addressing health disparities.

Summary of Research Completed

Specific Aim 1:

Longitudinal soluble receptor changes during uncomplicated pregnancy:

Our data collected during the first half of the funding period using gestational age-matched maternal plasma samples at mid-pregnancy and 3rd trimester, from women who later developed preeclampsia compared to uncomplicated (normotensive) pregnancy controls, suggested a decline in sc-kit (CD117, SCFsR) concentrations with advancing gestation. To demonstrate this directly, we assayed longitudinal samples collected at 4 gestational time points (weeks 5-10, 16-19, 27-30, and 40-42 (pre-delivery)) from 9 controls with uncomplicated pregnancy outcome. Clinical characteristics of these patients (who were different from those previously analyzed) are shown in Table 1. Plasma sc-kit, placental growth factor (PlGF, a pro-antiogenic factor decreased in preeclampsia) and soluble fms-like tyrosine kinase-1 (sFlt1, an anti-angiogenic factor increased in preeclampsia) were each measured by enzyme-linked immunoassay ELISA (R&D Systems) in duplicate on single plates. Data were analyzed by repeated measures ANOVA and Student-Newman-Keuls post-hoc pairwise comparisons. Relationships among these variables were assessed by Spearman rank correlation.

Figure 1 shows that sc-kit concentrations decreased progressively over the course of uncomplicated pregnancy. Significant decreases occurred at the 16-19-, 27-30- and 40-42-week compared to the 5-10 week intervals, and between the 16-19 and 40-42 weeks' gestation intervals (Figure 1). Figure 2 confirms previous reports that plasma PlGF increased during the first 30 weeks of gestation and then declines remarkably at term. Significant differences were found between the apparent apex at weeks' 27-30 and gestational weeks 5-10, 16-19 and 40-42. In contrast to sc-kit, sFlt-1 concentrations rose over the course of gestation, except for an apparent plateau at 27-30 weeks (Figure 3). Significant correlations between sc-kit and PlGF were observed at gestational ages 16-19 ($r= 0.70$, $P=0.03$) and 27-30 ($r=0.65$, $P=0.05$) but no other correlations of the three plasma variables within any of the other time points were observed. We are not aware of previous reports suggesting a relationship of these two angiogenic factors.

Further ELISA assay Validation:

Given that sc-kit levels decline with advancing gestation whereas sFlt-1 rises, we tested whether sFlt-1 interferes with the sc-kit ELISA. A pool of normal 3rd trimester pregnancy plasma (n=4 patients) with endogenous sc-kit concentration of 11.0 ng/mL was spiked (in two separate assays) with 0, 5000, 25,000 and 50,000 pg/mL human recombinant sFlt-1 (R&D Systems). Measured sc-kit concentrations in the spiked samples were 84, 100, and 86% of the unspiked sample, respectively, indicating no diminution in sc-kit values with increasing sFlt-1. We also performed spike-recovery tests on pregnancy plasma, comparing unspiked plasma with the same sample in which the concentration of sc-kit had been doubled by addition of recombinant sc-kit (R&D Systems). Recovery of spike ranged from 78.0 to 98.8 percent. Furthermore, we showed that 3 freeze-thaw cycles had no appreciable effect on measured plasma sc-kit levels.

We measured sc-kit using an ELISA from Cell Sciences (Cat # 850.700.192), using 9 control and 9 preeclampsia 3rd trimester cross-sectional samples previously used for measurement of sc-kit by the R&D ELISA. The Cell Sciences ELISA is claimed by the manufacturer to recognize both

natural and recombinant human soluble c-kit, but with much lower reported ranges. The correlation between the two ELISA kits, although positive, was poor Therefore, we plan to examine what distinguishes these two assays.

Specific Aim 3:
We recently became aware of data suggesting that the placenta is not a major source of circulating sc-kit compared to endothelial cells or mast cells. We thus first attempted to measure this soluble receptor in human umbilical vein endothelia cells (HUVEC, Lonza, Inc). *Method*: Passage 3 HUVEC were grown to ~75% confluence. The T75 culture plates were washed once with phosphate buffered saline (with calcium), and the cells refreshed by addition of phenol red-free endothelial basal medium (EBM; Cambrex Bio Science, Walkersville, MD) supplemented with EGM-2 SingleQuot supplements plus either 5% v/v or 0.1 % fetal bovine serum. Cells were maintained at 37°C in an atmosphere of 5% CO_2 for a total of 48 or 72 hours and then the conditioned media were harvested. Conditioned media were removed at the end of the time period, spun down to remove cells, and stored in 15ml conical tubes at -20C. On the day of the assay, media were thawed and concentrated 16-fold using Amicon Ultracel centrifugal filters with 30,000 molecular weight cut-off (cat# UFC803024). Sc-kit was measured by R&D ELISA on both concentrated and unconcentrated samples. A second series of experiments was performed in which conditioned media (EGM-2 plus 5% fetal bovine serum) were harvested after 4 hours treatment with phorbol ester (Sigma) [0ng/ml], [1ng/ml], [10ng/ml], and [100ng/ml], a manipulation reported to result in cleavage of membrane c-kit and thus production of sc-kit. *Result*: Unfortunately, none of the sc-kit values were appreciably above the detection threshold for the assay, and there were no detectable trends in the data.

We processed a material transfer agreement, and last week obtained an aliquot of HMC-1 cells (human mast cell line; Mayo Clinic Reference #MMV-88-049) as a kind gift from Joseph H. Butterfield, M.D., Mayo Clinic. HMC-1 is a unique human cell line that can serve as a resource for mast cell proteins including soluble receptors. The HMC-1 line was derived from a patient with mast cell leukemia and it is reportedly comprised of immature mast cells. HMC-1 cells lack a functional IgE receptor and have mutations in the coding sequence of the c-Kit proto oncogene, thus reportedly producing large quantities of sc-kit (Cruz AC et al. J Biol Chem 2004; 279:5612-5620). We are in the process of expanding these cells in culture. The cells, with and without small interfering (si)RNA blockade of c-kit synthesis, will be used to validate the ELISA assays, and to study circulating and placenta-derived factors from women with preeclampsia that may regulate shedding of c-kit from the cell surface of these HMC-1 cells in vitro.

We successfully filed a patent based on our pregnancy data, citing support from the Pennsylvania Department of Health, Commonwealth Universal Research Enhancement (C.U.R.E.) Program. This disclosure relates to using sc-kit predicting and diagnosing preeclampsia and eclampsia in pregnant subjects.
Pitt Ref. No. 02051
Klarquist Ref. No. 8123-83984-01
SOLUBLE CD117 (SC-KIT) FOR DIAGNOSIS OF PREECLAMPSIA AND ECLAMPSIA
Application No. 61/265,260, filed November 30, 2009

Table 1. Clinical Data of Longitudinal Normal Pregnancy Controls

	Normotensive Controls (n=9)
Age (years)	24.1 ± 6.1
BMI pre-pregnancy (kg/m^2)	26.1 ± 7.9
Gestational weeks at delivery	40.9 ± 0.6
Gestational weeks at venipuncture	
Sample 1	7.3 ± 1.8
Sample 2	17.7 ± 0.7
Sample 3	28.3 ± 0.8
Sample 4	40.8 ± 0.6
[#]Early pregnancy blood pressure:	
Systolic (mm Hg)	112 ± 6.8
Diastolic (mm Hg)	68 ± 6
Pre-delivery blood pressure:	
Systolic (mm Hg)	119 ± 17
Diastolic (mm Hg)	73 ± 4
Uric acid (mg/dL)	4.5 ± 0.9
Birth weight (grams)	3560 ± 540
Birth weight centile	51 ± 2
Race (% black)	33% (3/9)

Continuous variables are given as mean (standard deviation).
BMI, body mass index
[#] average of gestational blood pressures recorded before 20 weeks of gestation

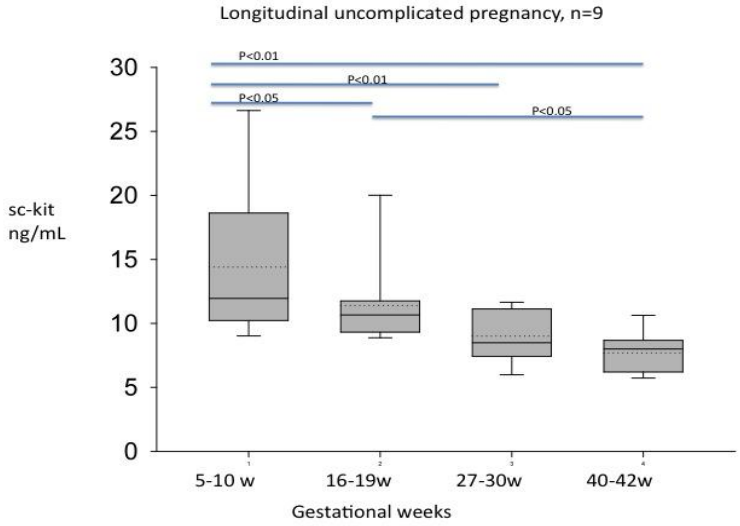

Figure 1. Box-plot of plasma sc-kit concentrations (y-axis) at successive gestational stages (x-axis) of uncomplicated pregnancy. The top, bottom, and solid line through the interior of the box correspond to the 75th percentile, 25th percentile, and 50th percentile (median), respectively. The whiskers (t bars) on the bottom and top denote the 10th percentile and 90th percentile, respectively. Dotted line denotes the mean. Significant differences are denoted by the horizontal lines above the boxes.

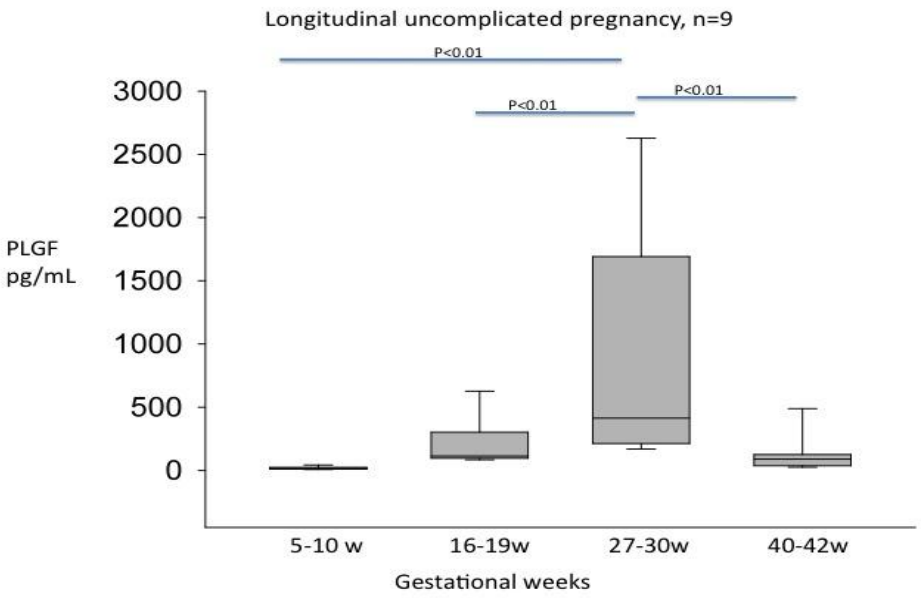

Figure 2. Box-plot of plasma placental growth factor concentrations at successive gestational stages of uncomplicated pregnancy. The top, bottom, and solid line through the interior of the box correspond to the 75th percentile, 25th percentile, and 50th percentile (median), respectively. The whiskers (t bars) on the bottom and top denote the 10th percentile and 90th percentile, respectively. Dotted line denotes the mean. Significant differences are denoted by the horizontal lines above the boxes.

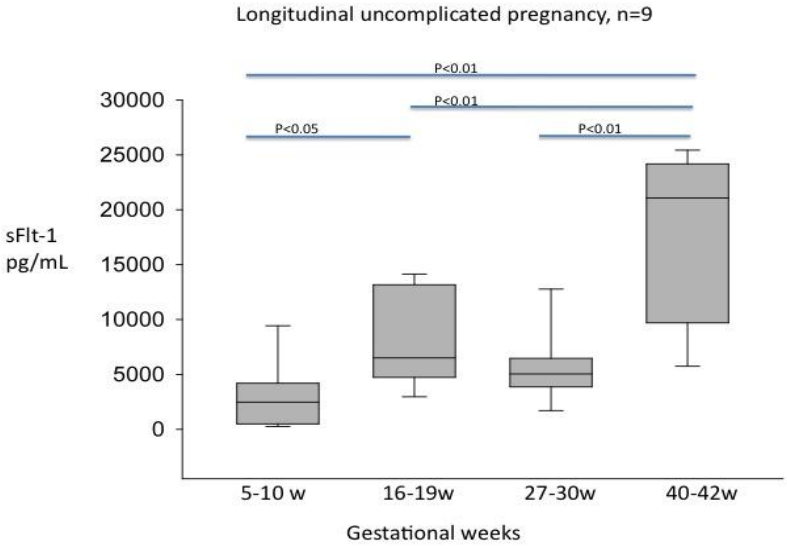

Figure 3. Figure 2. Box-plot of plasma fms-like tyrosine kinase-1 concentrations at successive gestational stages of uncomplicated pregnancy. The top, bottom, and solid line through the interior of the box correspond to the 75th percentile, 25th percentile, and 50th percentile (median), respectively. The whiskers (t bars) on the bottom and top denote the 10th percentile and 90th percentile, respectively. Dotted line denotes the mean. Significant differences are denoted by the horizontal lines above the boxes.

Research Project 6: Project Title and Purpose

Post-Transcriptional Regulation of Fstl1 mRNA in Human Trophoblasts - Our goal is to understand how cellular stress influences placental function, with its consequences on the developing fetus. Recently, we showed that oxygen deprivation alters the expression of many genes in the placenta, including genes that encode for microRNAs (miRNAs). The expression of one of these miRNAs, miR-198, is increased in hypoxia and is predicted to target the transcript for Fstl1. Suppression of Fstl1 could have important consequences for the placental function. In this project, we plan to investigate the influence of hypoxia on the post-transcriptional regulation of Fstl1 in the human placenta.

Duration of Project

1/1/2009 - 12/31/2009

Project Overview

1. Our research focuses on the molecular response of human trophoblasts to hypoxic stress. We have shown that hypoxia can alter the expression of numerous genes in trophoblast, including miRNAs. We recently performed several miRNA profiling experiments in human primary trophoblasts that were cultured in either standard oxygen conditions (FiO_2=20%) or in hypoxic conditions (FiO_2=1%). Using this approach, we identified miR-198 among a set of miRNAs that are differentially regulated in trophoblasts exposed to hypoxia. Interestingly, the gene encoding for miR-198 is nested within the transcription unit of the protein-coding gene Follistatin-like 1 (Fstl1). As a result of this structural organization, the expression of miR-198 is potentially linked to the transcription of Fstl1. Preliminary data showed a fairly high expression of Fstl1 mRNA in primary human trophoblasts. We also detected a reduction of Fstl1 expression in hypoxia. Examination of the 3'UTR of Fstl1 uncovered a target site for miR-198, and also revealed the presence of several sequence motifs that are known to mediate mRNA instability including AU-rich elements. This finding suggests that Fstl1 is post-transcriptionally regulated in human trophoblasts. Based on these observations, we hypothesized that placental Fstl1 is regulated by miR-198 and by the 3'AU-rich elements. To test this hypothesis, we generated two specific aims designed to assess the stability of Fstl1 mRNA in hypoxic trophoblasts: Correlate the expression of miR-198 with the production of Fstl1. We will determine whether the expression of miR-198 is linked to the transcription of Fstl1 and what are the consequences of increased miR-198 on Fstl1 protein output in primary trophoblasts exposed to hypoxia.
2. Analyze the posttranscriptional regulation of Fstl1 3'UTR. We will measure Fstl1 mRNA stability by blocking transcription with actinomycin D, and then we will dissect the role of the long AU-rich 3'UTR of Fstl1 in regulating protein stability.

Principal Investigator

Jean-François Mouillet, PhD
Research Instructor
University of Pittsburgh
Department of OBGYN and Reproductive Sciences
Magee-Womens Research Institute
204 Craft Avenue
Room A608
Pittsburgh, PA 15213

Other Participating Researchers

Yoel Sadovsky, MD - employed by University of Pittsburgh

Expected Research Outcomes and Benefits

Our long-term goal is to understand the response of the human placenta to injury, and in particular, to low oxygen (hypoxic) stress. This knowledge will pave the way for the design of new preventive measures to decrease the impact of placental injury on the developing fetus. Low placental oxygenation is one of the main stress conditions in the human placenta and is believed to play a role in the development of pathologies such as intrauterine growth restriction (IUGR) and hypertension of pregnancy. These conditions are associated with increased perinatal illnesses and mortality. Newborns surviving these insults are at risk for lifelong complications, including developmental diseases and a greater incidence of the adult metabolic syndrome (type-2 diabetes, high lipids, hypertension, obesity and related illnesses). Despite the well-documented association between hypoxia and these conditions, little is known about the mechanisms involved in the development of these defects.

Oxygen plays a major role in the differentiation of placental cells that occurs during pregnancy. We recently performed several experiments of placental cells cultured in low oxygen conditions to mimic placental hypoxia and examined changes in gene expression. This screen led to the identification of several genes including small RNA molecules (called microRNAs) whose expression is altered in hypoxia. In this project, we focus on a novel pathway of gene regulation in the human placenta, centering on regulation in the context of hypoxia. Results from our experiments are likely to advance our knowledge on previously unknown pathways that are activated during hypoxia and their role in placental response to injury.

Summary of Research Completed

This project was designed to investigate the intriguing association between the protein-coding gene Follistatin-like 1 (Fstl1), and miR-198 in the human placenta. The gene coding for mir-198 gene is located within the 3'UTR of the Fstl1 mRNA. Interestingly, the 3'UTR of Fstl1 also contains two potential binding sites for miR-198 suggesting a functional interaction between Fstl1 and miR-198. Little is known about the function and even the expression patterns of both

the protein FSTL1 and miR-198. Here, we analyzed the expression of both Fstl1 and miR-198 and their potential association in the human placenta.

In the six last months of funding for this project, we have made the following progress on the specific aims described in the original proposal:

Aim 1: Correlate the expression of miR-198 with the production of Fstl1.

Previous Northern blots analyses of Fstl1 and miR-198 in various cell lines and in primary trophoblasts revealed high accumulation of the Fstl1 transcript in primary trophoblasts while the miR-198 probe detected a unique pattern in trophoblasts. To further analyze miR-198 expression in the human placenta we performed *in situ* hybridization (ISH) on frozen sections using a DIG-labeled LNA probe. Fresh placental samples were pre-fixed in 4% paraformaldehyde (PFA) in PBS overnight, then in 0.5 M sucrose in PBS overnight and mounted in Tissue-Tek OCT (Sakura Finetek). Frozen sections (14 μm) were treated with 20 mg/ml proteinase K (Roche), then fixed in 4% PFA and acetylated for 10 min with a mixture of 0.25% acetic anhydride and 0.1 M triethanolamine. The postfixed tissues were subsequently incubated overnight with DIG-labeled LNA probes from Exiqon according to the manufacturer's instructions. After stringency washes, the slides were incubated with alkaline phosphatase conjugated anti-DIG antibody (Roche) and detected using BM Purple Substrate (Roche). Finally the slides were mounted in DPX (Fluka). Using this approach, we detected a strong signal in term placenta villi with a maximum intensity in the trophoblast layer and a weaker signal in the villous core.

We also used ISH to delineate Fstl1 mRNA expression in fresh placental tissue. Two anti-sense riboprobes specific to Fstl1 were produced and DIG labeled. One of the probes was ~700 nucleotides long and complementary to a region within the coding region of Fstl1. The other probe was ~600 nucleotides long and complementary to a region in the 3'UTR of Fstl1 (Fig. 1). Both probes gave a consistent signal in a sub-population of cells mainly located on the decidual side of the placenta (Fig. 1). Surprisingly, in contrast to the miR-198 probe, we did not detect any signal in the trophoblast layer. This result was unexpected because Northern blot assays had revealed a strong signal in isolated trophoblasts, only surpassed in intensity by HTR8/SV cells. The explanation for this apparent discrepancy is currently unknown. However, it is possible that our *in situ* hybridization protocol is not sensitive enough to detect Fstl1 expression unless highly expressed. Another potential explanation could be a difference in the accessibility of intracellular targets between the different cell types.

Next, we used immunohistochemistry to assess the FSTL1 protein in villous tissues. To confirm the identity of FSTl-expressing cells, we analyzed the expression of two markers of placental cell types: CD68 for Hofbauer cells and HLA-G for extravillous trophoblasts (EVTs). Slides with 5 μm paraffin sections were immunostained with a FSTL1 goat polyclonal antibody (R&D Systems, AF1694) or a CD68 mouse monoclonal antibody (DAKO, M0814). A monoclonal antibody MEM-G/9) (abcam ab7758) was used to detect HLA-G on frozen sections. Using this approach we detected a strong and specific expression of FSTL1 in EVTs. Although this result is consistent with the ISH staining, it does not fully resolve the apparent conflict between results obtained with ISH and Northern blot. Because the unique signal band observed in Northern blot

is of sufficient intensity and of the expected size (~4 kb), it is unlikely to result from non-specific hybridization. Therefore, we believe that Fstl1 mRNA is genuinely expressed in villous trophoblasts. The absence of FSTL1 immunostaining in villous trophoblast may be the result of insufficient sensitivity of the staining procedure or might result from translation inhibition. Further experiments are needed to resolve this issue.

Aim 2: Dissect the posttranscriptional regulation of Fstl1.

We first analyzed the effect of the Fstl1 3'UTR on the expression of a luciferase reporter in HTR8/SVneo cells. A miR-198-expressing vector was generated by cloning a DNA fragment containing the miR-198 precursor and flanking sequences as we have done for several miRNAs. For unknown reason this strategy failed to produce detectable level of mature miR-198 in transfected cells. We decided instead to transfect cells with a commercial miRNA oligonucleotide precursor or mimic (miRIDIAN microRNA Mimics, Dharmacon). To confirm the delivery and production of mature miR-198, we also generated a miR-198 sensor plasmid by cloning three artificial miR-198 response elements downstream of the Renilla luciferase gene in the psiCHECK^{TM}-2 vector (Promega). In HTR8/SVneo cells, the transfection of 50 nM of miR-198 mimic resulted in a potent inhibition of the miR-198 sensor reporter (>99% inhibition). In contrast, the miR-198 mimic had only a modest effect (~30% inhibition) on a reporter containing the 3'UTR of Fstl1. These experiments confirmed that transfection of a miR-198 mimic results in high delivery of a functional miR-198. Next, we tested these reporters in the context of primary trophoblasts after transfection with the DharmaFECT-Duo transfection reagent from Dharmacon. In primary trophoblasts, we detected a significant inhibition (60-70% inhibition) of the miR-198 sensor reporter; however, we did not observe any silencing of the Fstl1 reporter construct. These data suggest that Fstl1 transcripts are probably not regulated by miR-198 in trophoblasts.

Sequence analysis of Fstl1 3'UTR revealed the presence of multiple copies of the signature motif AUUUA or AU-rich elements (AREs), which are elements promoting mRNA instability. We then used our luciferase-based reporter assay to study the regulation of Fstl1 by its 3'UTR sequences. For this, a series of truncations was designed to remove segments of the Fstl1-3'UTR containing sequence features such as AU-rich elements but also the sequence coding for miR-198 as well as the potential miR-198 binding elements (Fig. 2). In addition to primary trophoblasts, we performed these experiments in two trophoblast-derived cell lines: BeWo cells and HTR8/SVneo cells. The results display widely fluctuating luciferase activity in the different cell types. Furthermore, deletions also produced significant alterations of the luciferase activity. Yet, these experiments revealed a complex situation in which several regions are likely to be important for the regulation of the activity of the transcript. One limitation of this approach is that truncations may alter the overall conformation of the 3'UTR and compromise the potential binding of regulatory RNA binding proteins mediating the decay or increased stability of the transcript. An alternative will be to create point mutations in individual AU-rich elements.

To further analyze the downregulation mediated by Fstl1 3'UTR in primary trophoblasts we investigated the stability of the endogenous Fstl1 mRNA after treating the cells with the transcription inhibitor actinomycin D (ActD). Primary trophoblasts were cultured in standard oxygen concentration (FiO_2 = 20%) or reduced oxygen (FiO_2 = 1%) then exposed to 5 μg/μl of

ActD. Cells were harvested at 0, 2, 4, 6, 8, 12 and 24 hours after treatment and total RNA from each time-point was isolated with Tri-Reagent (MRC). Real-time PCR was performed on a 7900HT Fast Real-Time PCR system (Applied Biosystems) using SYBR green chemistry. Surprisingly, we found that Fstl1 mRNA was very stable both in normal and hypoxic conditions. Even 24 hours after exposure to ActD there was hardly any difference at the level of Fstl1 mRNA measured by real time PCR. The amount of total RNA extracted after 12 and 24 hours of treatment with ActD was sharply reduced, which shows that transcription inhibition was effective. Although we cannot rule out a transcriptional effect to explain the observed reduction of Fstl1 mRNA in hypoxic trophoblasts, we can also imagine a blocking of Fstl1 mRNA translation. A translational effect would also explain the absence of FSTL1 protein in the villous trophoblasts despite the presence of the corresponding mRNA, which was detected by Northern blot.

Tables, Figures and Legends

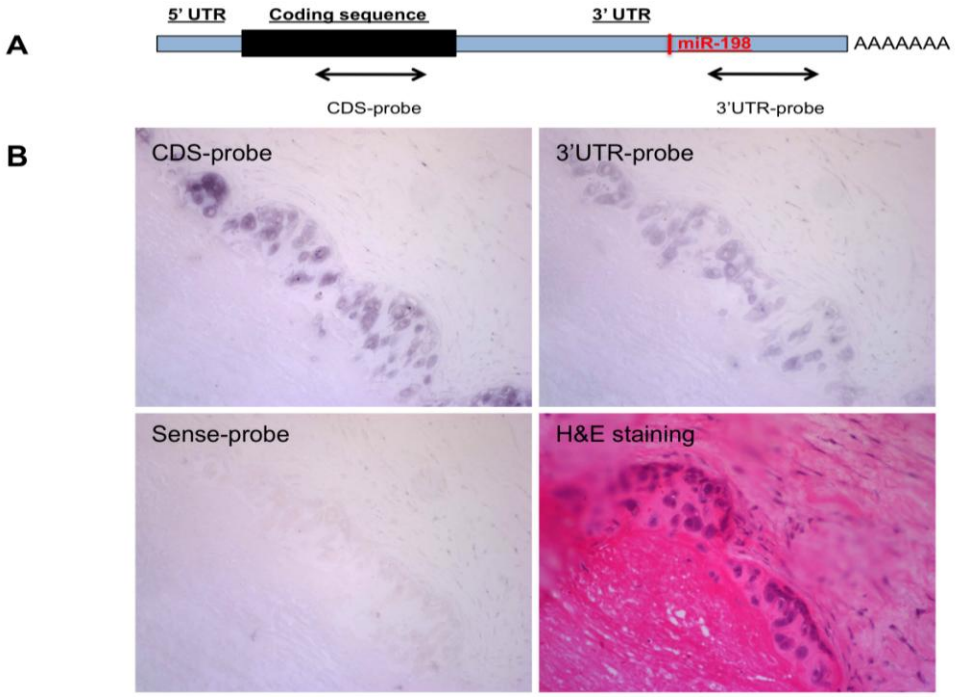

Fig. 1: Pattern of FSTL1 expression in the human placenta, revealed by RNA *in situ* hybridization. A: Schematic representation of the Fstl1 transcript with the localization of the probes used for ISH. B: Expression of Fstl1 was detected in extravillous trophoblasts (EVTs) using two different RNA probes located in the CDS (top, left panel), and in the 3'UTR of Fstl1 (top, right panel). Also shown is a section stained with a control sense probe (bottom, left panel), and with hematoxylin-eosin staining (bottom, right panel). Original magnification = X200

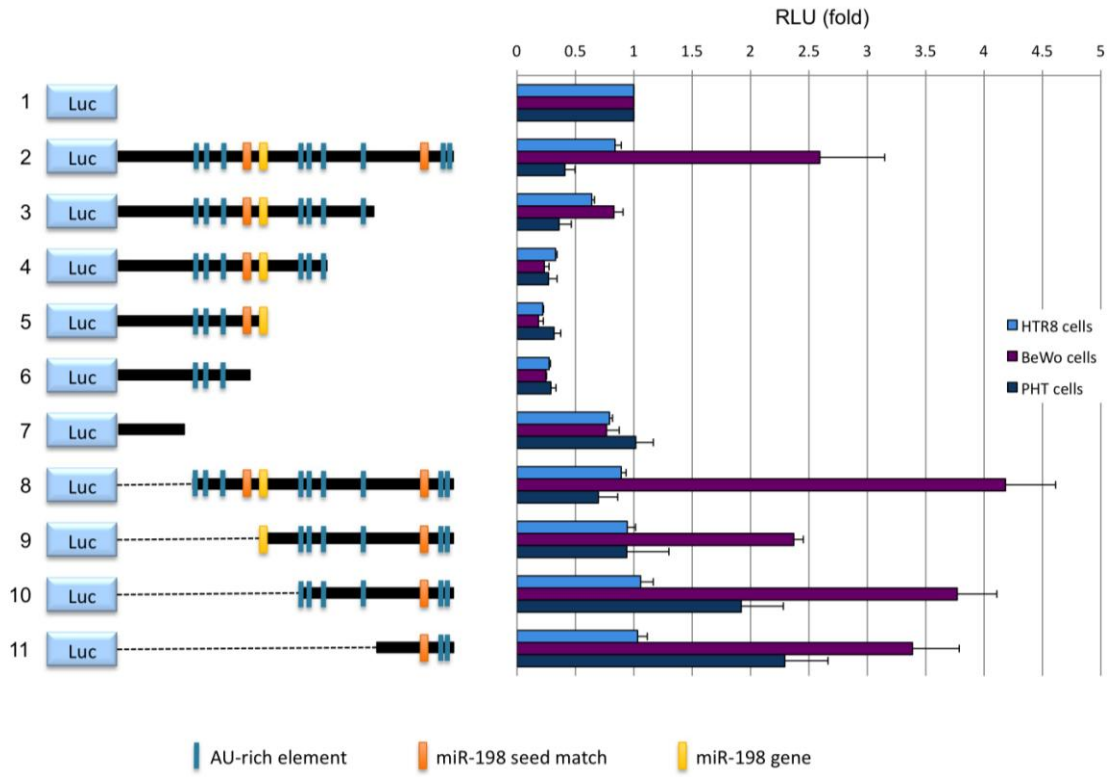

Fig. 2: The 3'UTR of Fstl1 contains regions that influence the stability of the luciferase transcript. Various truncations of the Fstl1 3'UTR were generated and cloned downstream of the *Renilla* luciferase from the psiCHECK-2 vector. As a control, we used the empty psiCHECK-2 plasmid. Each construct was transfected in HTR8/SVneo cells, BeWo cells or primary trophoblasts (PHT). Luciferase activity was determined 48 hours after transfection. Relative luciferase unit (RLU) activity from the control reporter construct was set at 1. *Renilla* luciferase activity was normalized to firefly luciferase.

Research Project 7: Project Title and Purpose

Analysis of Functional Domains within NDRG1 - Our research goal is to improve pregnancy outcome and allow the developing fetus to reach its full developmental potential. This project centers on the placenta, a "sole-source" provider of oxygen and nutrients to the developing fetus. Decreased supply of oxygen (hypoxia) is a common pathway for many injuries that may affect the placenta. We focus our research on a protein (NDRG1) that we have identified as a critical regulator of placental adaptation to hypoxia. While it is known that NDRG1 diminishes placental injury and cell death in response to hypoxia, we do not understand how NDRG1 works. We propose to dissect the mechanism of action of NDRG1 in placental cells. This will allow us to control the action of this protein, which may pave the way to new tools designed to improve placental function, and consequently, fetal health.

Duration of Project

1/1/2009 - 12/31/2009

Project Overview

This project centers on a protein called N-myc downstream regulated gene 1 (NDRG1), which plays an important role in regulation of cell proliferation, differentiation and apoptosis in diverse cell types. In several types of cancer cells, NDRG1 reduces the rate of cell proliferation and promotes programmed cell death. NDRG1 is also important in the function of Schwann cells. In our laboratory we found that NDRG1 expression is markedly increased in placental trophoblast cells that are exposed to hypoxia. Importantly, using lentivirus-mediated over-expression of NDRG1, we showed that NDRG1 attenuates hypoxic injury in primary human trophoblasts. As expected, silencing of NDRG1 in primary human trophoblasts led to enhanced hypoxia-induced apoptosis.

Although pertinent to several cellular processes, the mechanism of action of NDRG1 remains unknown. Computerized analysis suggested that NDRG1 belongs to a family of protein hydrolases, yet it lacks a hydrolase activity. This application serves as a first attempt to dissect the function of putative domains within NDRG1. In this grant project we hypothesize that discrete domains within NDRG1 determine the function of this protein in cellular differentiation and apoptosis. We will (a) use deletion mutagenesis to create NDRG1 proteins that are deficient in discrete domains, and assess their influence on cell proliferation in a cell line, and (b) dissect the specific functions of identified NDRG1 domains in the context of primary human trophoblasts.

Our research targets the function of NDRG1 primarily in human trophoblast. Understanding the function of NDRG1 in the placenta will illuminate pathways that underline placental adaptation to injury. Placental dysfunction is the most important cause of fetal growth restriction, a disease associated with increased perinatal morbidity and mortality. Moreover, surviving children are susceptible to cerebral palsy and growth delay, and as adults they are at greater risk for acquiring metabolic syndrome. Lastly, while our research targets the placenta, results from our proposed experiments have a direct relevance to cancer and attenuation of tumor growth.

Principal Investigator

Yoel Sadovsky, MD
Professor and Vice Chair (Research)
University of Pittsburgh
Magee Womens Research Institute
204 Craft Avenue
Room A608
Pittsburgh, PA 15213

Other Participating Researchers

Xiao-Hua Shi, MD, MS - employed by University of Pittsburgh

Expected Research Outcomes and Benefits

Our goal is to understand mechanisms that govern placental response to insults that might occur during pregnancy. Such insults can lead to fetal growth restriction, which causes early neonatal morbidity and mortality, and is implicated in developmental delay and neurological dysfunction during childhood. Furthermore, inadequate fetal growth has been recently associated with the adult "metabolic syndrome," a cluster of disorders during adult life, including type-2 diabetes, hypertension, heart disease, hyperlipidemia and obesity. Intact fetal growth depends on placental function at the fetal-maternal interface, including gas exchange, supply of nutrients and removal of waste products. Diverse types of physical, chemical and biological insults may adversely influence the balance between placental cell injury and repair, resulting in substandard fetal growth.

As a part of our efforts to advance our knowledge of mechanisms that underlie placental injury and adaptation, we identified a protein that functions to attenuate placental cell injury in response to hypoxia. This protein, called NDRG1, improves placental cell function and reduced cell death. Importantly, this protein is also expressed in a number of human cancers, where it decreases the rate of cell proliferation. While clearly important, we do not understand how this protein works. This project outlines our initial attempt to dissect the mechanism of action of NDRG1. Our study will illuminate molecular targets that are directly influenced by NDRG1, and therefore highlight the means to regulate NDRG1 activity. Information gleaned from our experiments will pave the way to research on previously unrecognized ways to improve placental function and hence, fetal health. Our results may also shed light on cancer biology, and on reduction of tumor growth.

Summary of Research Completed

<u>Aim I: Create mutations within N-myc downstream regulated gene 1 (NDRG1) protein and assess their influence on proliferation in a cell line.</u>

During the recent six months constituting the latter half of the funding period, we advanced the experiments described in this Aim, achieved key goals, and expanded our pursuits in order to advance the science and solidify our conclusions.

As discussed in our original application, we thoroughly analyzed putative functional domains within NDRG1, and examined the evolutionary conservation as well as the conservation of these domains in other members of the NDRG family. Based on our analysis in the first 6 months of the project, we created mutations in the following NDRG1 domains: (1) NDRG1del$_{2\text{-}42}$, which is deleted for a large portion of the N-terminus (including the putative DNA-binding domain), (2) NDRG1del$_{21\text{-}42}$, which is deleted for the helix-turn-helix putative DNA-binding domain at the proteins N-terminus, (3) NDRG1del$_{1\text{-}317}$, which is deleted for NDRG1 unique C-terminus (including several phosphorylation sites), and NDRG1del$_{339\text{-}368}$, which is deficient in the three C-terminal repeats. During the recent funding period we have added an additional mutation, which deletes the phosphopantetheine attachment site (PPAS), located at aa 128-143. This domain serves as a potential nuclear localization signal, and is conserved in several acyl carrier proteins, including fatty acid synthase, where it serves as a "swinging arm" for the attachment of

activated fatty acid and amino acid groups. Akin to the other mutants, we cloned this truncated form of NDRG1 (using a two-step PCR approach as described in our previous progress update) into a pcDNA 3.1a vector upstream from a C-terminal myc-tag, designed to enable detection of the mutant NDRG1 protein and distinguish it from the endogenous, untagged protein.

In addition to the effect of NDRG1 on proliferation, we elected to advance our studies and develop several other physiological assays, with the goal of improving our ability to uncover the function of NDRG1 in trophoblasts. Similar to the assessment of the activity of caspase 3, a key mediator of apoptosis, as an effective tool in uncovering the function of NDRG1 in hypoxia, we found that exposure of trophoblasts to injury by ultraviolet (UV) light enhanced apoptosis (determined by increased caspase 3 activity). Importantly, we found that the over-expression of wild-type NDRG1, but not NDRG1 in which the N-terminus or the helix-turn-helix (HTH) domains (both deficient in the HTH domain), attenuated this effect. These results support the significance of the N-terminal domain for the function of NDRG1, and pave the way to additional detailed experiments designed to pursue the function and potential targets for that domain. The function of the other mutants in trophoblast hypoxic response or in response to UV light is currently pursued in our lab.

Aim II: Test for specific functions of the identified NDRG1 domains in primary human trophoblasts.

Because one of the main functions that we planned to assess in primary human trophoblasts was differentiation, not cell proliferation (primary human trophoblasts do not proliferate in vitro), we analyzed the effect of NDRG1 inhibition on cell differentiation, which is one of the characteristic features of primary human trophoblasts that are cultured for 72 hours. This analysis was initially performed in the trophoblast line BeWo. BeWo cells are an excellent model for trophoblast differentiation, because these cells differentiate in response to addition of either forskolin or cAMP to the culture medium. As seen in Fig. 1, we successfully silenced NDRG1 in BeWo cells and showed that decreased NDRG1 expression attenuated the release of hCG, a marker of cell differentiation, to the culture medium.

Because intracellular localization of NDRG1 was markedly altered by hypoxia in trophoblast cell lines, we sought to assess whether or not this was reproducible in primary human trophoblasts, which form multinucleated syncytia as they differentiate in vivo and in vitro. Primary human trophoblasts were exposed to hypoxia in our hermetically enclosed hypoxia chamber. After 24-72 hours the cells were fixed with 4% paraformladehyde for 30 min, blocked with 0.1% BSA and then permeabilized with 0.1% Triton X 100. We performed immunofluorescence using a rabbit anti-NDRG1 polyclonal antibody (Zymed) followed by cell incubation with an Alexafluor 488-linked goat anti-rabbit antibody. The images were captured with an Olympus AX70 Provis fluorescence microscope, equipped with an Olympus Fluoview 1000 confocal imaging system. As shown in Fig. 2, exposure of primary human trophoblasts to hypoxia for 24-72 hours resulted in altered intracellular expression of NDRG1, with enhanced localization of NDRG1 to the nucleus and a concomitant decrease in cytoplasmic expression of NDRG1. These changes were not observed in cells exposed to standard conditions (not shown).

We used two approaches to further quantify nuclear localization of NDRG1. First, we counted the number of nuclei that expressed NDRG1. For that purpose, we transfected JEG3 cells with an NDRG1 expression vector and counted the number of NDRG1-positive cells in cells exposed to the hypoxia-mimetic cobalt chloride (CoCl) vs. control. As shown in Fig. 3A, cells exposed to CoCl exhibited greater nuclear localization of NDRG1 than control cells. This was quantified as shown in Fig. 3B, which revealed a greater fraction of NDRG1-positive nuclei in exposed trophoblasts. In a second approach, we used cell fractionation and extracted nuclei and cytoplasm fractions from cells cultured in normal condition, hypoxia, or from cells treated with CoCl. We examined NDRG1 expression in these fractions using western immunoblotting. Consistent with our staining analysis, we found that the expression of NDRG1 in the nuclear fraction was significantly increased in cells exposed to $CoCl_2$ or incubated in hypoxia (FiO_2 <1%) for 24 hours (Fig. 4).

Finally, in the last report we discussed our use of lipofection in order to express proteins (or lentivirus expression vectors) in trophoblasts. Because our results highlighted the need to simultaneously silence endogenous NDRG1 (using siRNA) while overexpressing exogenous wild-type or mutant NDRG1, we elected to test the use of DharmaFECT-2 (Dharmacon). This reagent is designed for co-expression of short silencing oligonucleotide along with a protein-encoding expression vector. We tested this approach in our cell system using transfections in 6-well plates with antibiotic-free medium, and found it to be very effective. Importantly, in repeated experiments we did not detect any evidence for cell toxicity. This therefore has become our working tool while we deploy a lentivirus system in primary trophoblasts.

Overall, we believe that the experiments supported by the latter six months of funding advanced our knowledge on the function of NDRG1 during trophoblast adaptation to injury. Our results validated the necessary technologies and served to define molecular functions that are directly influenced by NDRG1. We believe that understanding the molecular actions of NDRG1 will shed light on means to regulate the activity of this important protein.

Figures

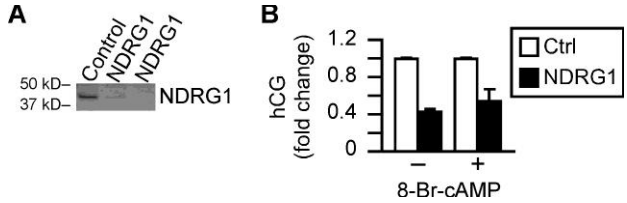

Fig. 1: Silencing of NDRG1 attenuates differentiation of BeWo cells. A) Two different NDRG1 siRNA constructs were effective in silencing NDRG1 expression. B) The effect of NDRG1 silencing on hCG release in BeWo cells in the absence or presence of 8-Br-cAMP (0.5 mM for 24 h).

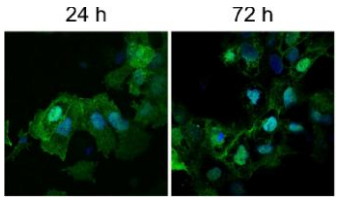

Fig. 2: Hypoxia enhances nuclear localization of NDRG1 in primary human trophoblasts. Trophoblasts were cultured in standard (FiO_2=20%) or hypoxic (FiO_2=1%) atmosphere for 24-72 h, and NDRG1 detected as described in the text. Nuclei (blue) were visualized with Hoechst 33342.

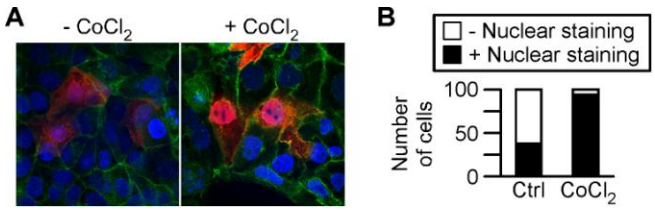

Fig. 3: Exposure to cobalt chloride (CoCl) enhances nuclear localization of NDRG1. A) JEG3 cells were transfected with myc-tagged NDRG1 and cultured in CoCl (200 microM for 24). NDRG1 (red) was detected using an anti-myc antibody, cell membranes were detected using an anti-E-cadherin Ab, and nuclei (blue) were visualized with Hoechst 33342. B) The number of NDRG1-positive nuclei was quantified as described in the text. The difference between the paradigms was significant ($p < 0.05$).

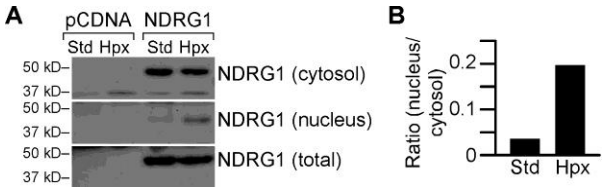

Fig. 4: The effect of hypoxia on the expression of NDRG1 in isolated nuclei. A. Cellular nuclei and cytoplasm were isolated, and NDRG1 levels were determined by western immunoblotting. Tubulin (expressed in cytoplasm) and Lamin A/C (expressed in nuclei) served as control. B. quantified analysis of nuclei/cytoplasm NDRG1 expression ratio.

Research Project 8: Project Title and Purpose

Immunity to MUC1 Tumor Antigen in Conditional and Transplantable in vivo Models for Ovarian Cancer - Ovarian cancer is the most lethal gynecologic cancer. Standard treatment for this disease begins with surgery followed by chemotherapy. However, these approaches are often ineffective, thus raising the need for new and improved therapies. The patient's immune system has the ability to recognize antigens on tumor cells and to eliminate them, making immune therapy with cancer vaccines an attractive approach for adjuvant therapy. The design and implementation of tumor antigen-based vaccines requires adequate in vivo animal models. In this project, we will generate two in vivo mouse models that express the tumor antigen MUC1, a cancer vaccine candidate. Using these complex models we will study how the immune system recognizes the antigen during ovarian cancer progression, with consequences on future cancer vaccine design.

Duration of Project

1/1/2009 - 12/31/2009

Project Overview

Despite progress in therapy, ovarian cancer continues to be associated with high mortality rate, and is the most lethal gynecologic cancers. The lesions are thought to originate in the ovarian surface epithelial (OSE) cells, although the disease pathogenesis is not well understood. The OSE in humans express low levels of MUC1 glycoprotein; in contrast, the epithelial tumors derived from them overexpress a modified form of MUC1. Because the immune system of

ovarian cancer patients can recognize MUC1 when expressed by tumors, MUC1 has been considered a tumor-associated antigen and shows promise as a cancer vaccine candidate. However, the biology of this antigen and its immunogenicity during natural progression to ovarian cancer is not well understood and requires adequate in vivo animal models, which we aim to generate here.

By combining mouse genetics and survival surgery in mice, we propose the following specific aims:

Aim 1. To generate and characterize a conditional, triple transgenic mouse model for ovarian endometrioid ovarian cancer. These mice will express the mutated KrasG12D oncoallele, are homozygous for the Pten deletion and express the human MUC1 antigen ($MUC1^{+/-}$LSL-$Kras^{G12D/+}Pten^{loxP/loxP}$). We postulate that these mice will progress to MUC1-expressing endometrioid ovarian cancer, via induction with Cre-lox system. The tumors will develop in the ovaries and will spread to the peritoneal cavity, similarly to the human disease.

Aim 2. To generate and characterize a syngeneic, transplantable ovarian tumor model expressing MUC1.

The mice will be injected IP with a syngeneic ovarian epithelial cell line generated from MUC1 transgenic mice (called MKOSE). We postulate that the mice will develop MUC1-expressing tumors in the peritoneal cavity, mimicking the recurrence associated with late stage disease seen in humans.

Aim 3. To assess MUC1 expression and immunogenicity changes in mice either progressing to ovarian cancer or with transplantable IP tumors. We postulate that the $MUC1^{+/-}$LSL-$Kras^{G12D/+}Pten^{loxP/loxP}$ mice with induced tumors will show increasing MUC1 expression in the ovaries, will develop MUC1-specific IgG antibodies and will show Treg accumulation in regional lymph nodes and in ascites similar to humans. The MKOSE-injected mice will lack tumors in the ovaries and will show similar phenotype.

Characterization of these two models will enable us to later develop and test in vivo MUC1 cancer vaccines.

Principal Investigator

Anda M. Vlad, MD, PhD
University of Pittsburgh School of Medicine
Magee Womens Research Institute B403
204 Craft Avenue
Pittsburgh, PA 15213

Other Participating Researchers

Raluca Budiu, PhD - employed by University of Pittsburgh

Expected Research Outcomes and Benefits

Although ovarian cancer responds well to chemotherapeutic drugs, tumors often recur and reintroduction of chemotherapy predictably leads to a response that is short lived when compared to the response seen with initial therapy. The disappointing overall survival gains can be explained by the inability of current approaches to eradicate the residual disease, therefore new

and improved therapies are needed. Active immune therapy with cancer vaccines holds promise and is currently tested in numerous, worldwide clinical trials. Studies to date demonstrate that immune cells are recruited to developing solid tumors, where complex immune-tumor cell interactions take place. Most effective against tumors are mechanisms of adaptive immunity (called T and B lymphocytes and their secreted factors) which can detect the tumor cells in a highly specialized manner. Boosting these mechanisms with vaccines may provide benefit for the host in fighting off the tumor recurrence. The best way to vaccinate in solid tumors (including ovarian cancer) still needs to be defined and the success rate in this research area may ultimately depend on generating animal models relevant for the human disease and in which vaccines can be tested and perfected. One vaccine candidate currently tested in clinical trials is MUC1 tumor-associated antigen. The two models we propose to generate here are novel and offer several significant advantages over the currently available in vivo models. The transplantable model uses a cell line we derived from MUC1 Tg mice. We postulate that injection of the transformed cells in the peritoneal cavity leads to the formation of MUC1+ tumors. The conditional model takes advantage of the Cre-lox technology and uses mice progressing to MUC1-positive ovarian tumors which also spread in the peritoneal cavity. These transgenic mouse models mimic late stage ovarian cancer and will help us study ovarian cancer pathogenesis and immune system-tumor cell interactions. In the long run, generation and identification of these mice will be instrumental for further studies on MUC1-based immune therapies in ovarian cancer.

Summary of Research Completed

Rationale. Ovarian cancer has the highest fatality rate of any gynecologic malignancy and is the fourth leading cause of death in women. Advances in novel therapeutic approaches require new and improved animal models. Most animal models to date use xenograft and/or orthotopic implantation of human tumor cell lines in immunocompromised mice. These models, however, are unsuitable for studies on immune regulation and thus with limited usefulness for clinical trials with immune biologics.

Genetically engineered mouse models have become more valuable in vivo systems for understanding molecular mechanisms of tumorigenesis and for defining better therapeutic agents. By combining mouse genetics and survival surgery in mice, we proposed here to generate a triple Tg mouse model progressing to human MUC1-positive ovarian tumors.
MUC1 is overexpressed in all histological types of ovarian tumors and because the immune system of ovarian cancer patients can recognize MUC1 on ovarian cells, MUC1 has been considered a tumor-associated antigen and shows promise as a cancer vaccine candidate. Furthermore, MUC1 is an oncoprotein with important roles in transformation, migration and metastasis. However, changes in MUC1 biology and immunogenicity during natural progression to ovarian cancer have not been addressed and a better understanding of MUC1 roles requires adequate in vivo animal models. Our proposed aims and research accomplishments are detailed below.

Research progress.

Aim 1. To generate and characterize a conditional, triple transgenic mouse model for ovarian endometrioid ovarian cancer.

In order to obtain triple Tg mice, we implemented complex mouse breeding protocols, using previously generated, as well as newly derived, single and double transgenic mice.

The rationale of the mouse breeding regimen was described in the original application and detailed in the previous progress report.

Selection of pups heterozygous for the MUC1 and KrasG12D transgenes and homozygous for floxed Pten (triple Tg MUC1KrasPten mice), was performed by PCR using tail-extracted DNA, as detailed in our application.

After confirming the phenotype previously reported by Dinulescu et al in the KrasPten mice (Fig. 1), we next used the newly obtained triple Tg mice for AdCre injection during survival surgery. Similarly to results from double Tg mice, all the injected, triple Tg MUC1KrasPten mice developed tumors, confirming the 100% disease penetrance. We sacrificed the diseased mice and harvested at necropsy the ovarian as well as other abdominal tumors, diaphragm, lungs, liver, pancreas and kidneys. All tissues were formalin-fixed and embedded in paraffin. Four micron sections were subjected to immunohistochemistry (IHC) staining. All tumor sections from triple and double (control) Tg mice were subjected to IHC staining for the following markers: MUC1, cytokeratin 7, estrogen receptor (ER), pErk, pMEK, snail, WT1.

We report below a list of similarities and differences from double triple Tg mice.

Similarities:
1. The tumors in both double and triple Tg mice were accompanied by hemorrhagic ascites and numerous metastases in the peritoneal cavity and on the diaphragm (Figures 1 and 2), mimicking the biology of late stage human tumors.
2. The hematoxyllin-eosin (HE) staining showed similar histology in the triple and double Tg tumors (Fig.1 and 2). However, as expected, MUC1 was present in the triple Tg tumors only (Fig. 2).
3. Both double and triple tumors were cytokeratin 7 + and showed increased pMEK and pERK by IHC, consistent with the enhanced signaling via the Kras and Akt pathways in these genetically engineered mice (not shown).

Differences:
1. The triple Tg mice developed tumors with a higher kinetics (average of 37 in triple Tg versus 77 days in double Tg mice, $p<0.05$), suggestive of a more aggressive phenotype in mice carrying the transgene encoding for the human MUC1-associated antigen, a known oncoprotein involved in cell transformation.
2. Our IHC results with an antibody that stains both murine Muc1 and human MUC1 cytosolic tail (CT) show low/no mouse Muc1 in double Tg ovarian surface epithelium (OSE, Fig. 3C) and

double Tg ovarian tumors (Fig. 3E). However, CT2 staining is positive in endometrial glands (Fig 3A, B), demonstrating the ability of CT2 antibody to properly identify positive cells. Furthermore, unlike the double Tg tumors, the triple Tg ovarian tumors were CT2 positive, given the presence of the MUC1-associated CT epitopes (Fig. 3F).

In summary, after completing aim 1, we were able to generate and characterize a triple transgenic, human MUC1 antigen-expressing ovarian cancer mouse model. These mice progress to tumors with a human-like biology and express the human MUC1 tumor-associated antigen, mimicking even closer the human disease. The mice reported in these studies will greatly advance our capacity to address important questions in the future related to ovarian tumor pathogenesis and to monitor preclinical testing of novel MUC1-based immune therapeutics.

Aim 2. To generate and characterize a syngeneic, transplantable, MUC1-expressing ovarian tumor model.

To complete this aim we used a syngeneic ovarian tumor cell line IG10 which we transfected with a MUC1-encoding plasmid. The newly obtained IG10-MUC1 cells expressed high MUC1 levels (in line with levels seen in human ovarian cancer lines, not shown) and were able to generate MUC1+ tumors in vivo. Numerous tumors were visible throughout the peritoneal cavity, ranging in size from 1 mm to 5-6 mm. The tumors were accompanied by hemorrhagic ascites, a profile similar to the one observed in some of the conditional mice with tumors Fig 4**.** However, unlike the tumors developing in the double and triple Tg mice, the transplantable IG10-MUC1 tumors have undefined histology (Fig 4 E and F). Importantly, however, the tumors maintained MUC1 expression in vivo (Fig. 4F) and are adequate models for studies on MUC1 specific immunity in transplantable ovarian tumors.

Our results from aim 2 show that despite several limitations, our newly developed transplantable model based on IP injection of IG10-MUC1 is the only one currently available for MUC1 studies in immune competent mice with transplantable ovarian tumors expressing a human tumor antigen and therefore constitutes a resourceful tool for future preclinical studies on natural and vaccine-induced MUC1-specific immunity in ovarian cancer.

Aim 3. To assess MUC1 expression and immunogenicity changes in mice either progressing to ovarian cancer or with transplantable IP tumors.

After having observed considerable increases in tumor MUC1 expression by IHC, we also addressed the possibility of soluble MUC1 detection in serum of triple Tg, tumor-bearing mice. When overexpressed, MUC1 can also be cleaved off the tumor cell membrane and released into the circulation. However, despite increases in soluble serum MUC1 by CA 15-3 test in 50% of the tumor-bearing mice, the antibody ELISA measurements showed that no detectable IgM or IgG MUC1-specific antibodies could be identified at any time before or after tumors occurred (Fig .5). This lack of MUC1-specific humoral immunity may be explained by increased immune suppression in the host.

To address this, we explored the extent of immune suppressive T cell (Treg) accumulation in the spleen and regional lymph nodes of tumor-bearing mice. Our results show a dramatic increase in

Treg population in the secondary lymphoid organs (where 5-8% Treg are expected), similar to reports from cancer patients. Similar increases were also noted in triple Tg tumor-bearing mice (not shown).

Interestingly however, despite significant increases in Treg percentages in tumor bearing double and triple Tg mice over healthy controls, we could not detect any significant differences in Treg percentages in triple versus double Tg mice.

Overall, these results suggest that although increased Treg percentages may be responsible for the lack of spontaneous humoral immunity against the MUC1 antigen, they are not responsible for the more aggressive phenotype seen in triple Tg mice. Our future studies will focus on the identification of MUC1-mediated mechanisms involved in the accelerated tumor progression of triple Tg mice.

Figures and Legends.

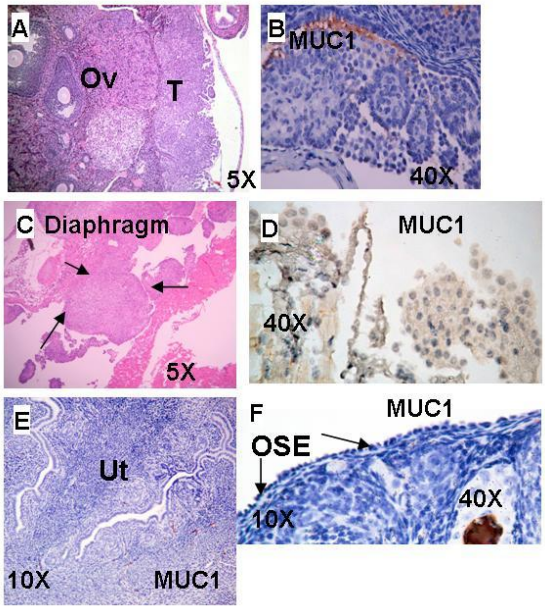

Fig. 1. Phenotype of double Tg (KrasPten) mice injected in the ovarian bursa with Cre-encoding adenovirus, during survival surgery. The tumors developed in 100% of the injected mice, after an average of 11 weeks post-disease induction. (A) The hematoxyllin-eosin (HE) staining shows tumor extent (T). The tumors show endometrioid histology and are MUC1 negative (B), as expected. Metastatic tumors occur often on the diaphragm (C). The MUC1 negative staining in the uterus and ovarian surface epithelium (OSE) in healthy mice are shown in E and F, respectively.

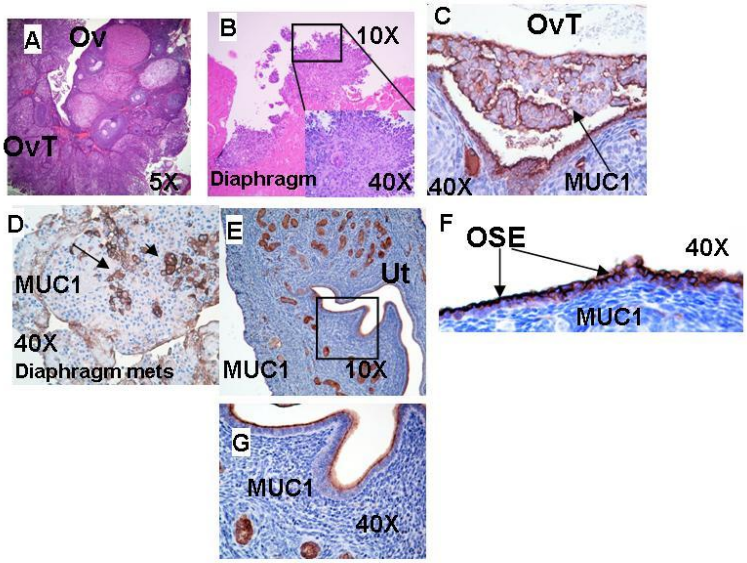

Fig. 2. Phenotype of triple Tg (MUC1KrasPten) tumors The tumors developed in 100% of the injected mice, after an average of 5 weeks post-disease induction (A). The tumors show endometrioid histology and are MUC1 positive (C). Metastatic tumors occur often on the diaphragm (B) and are also MUC1 positive (D). The MUC1 positive staining in the uterus and ovarian surface epithelium (OSE) in healthy mice are shown in E and F, respectively. Image in G is a magnification of the detail (box) in E.

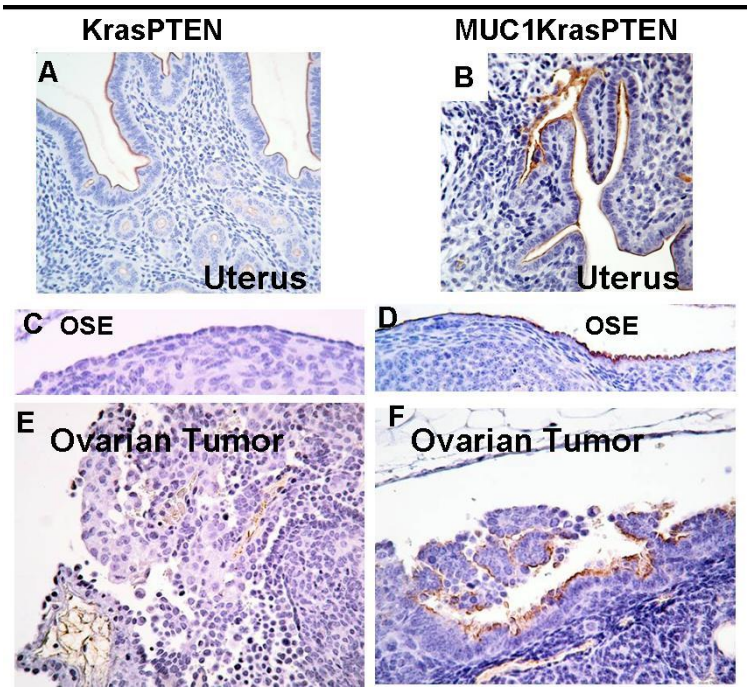

Fig.3. Detection of mucin 1-cytosolic tail (CT) in tissues from double (A,C,E) and triple (B,D,E) transgenic mice by IHC. Staining was performed with a monoclonal antibody (clone CT2) that detects MUC1-CT as well as Muc1-CT. Staining patterns seen in the uterus (A,B) ovarian surface epithelium (OSE, C,D) and ovarian tumors (E,F). In double Tg mice CT2 antibody detects Muc1-CT while in triple Tg mice CT2 detects both murine (Muc1-CT) and human (MUC1-CT) molecules. These results suggest that in double Tg mice (A, C, E), the endogenous (murine) mucin1 is present in the uterine glands (A), but absent from the OSE (C) and from the ovarian tumors (E). In contrast, when human MUC1 is present as a transgene (B, D, F), the CT2 antibody stains not only the uterine glands (B) but also the OSE (D) and the ovarian tumor (F).

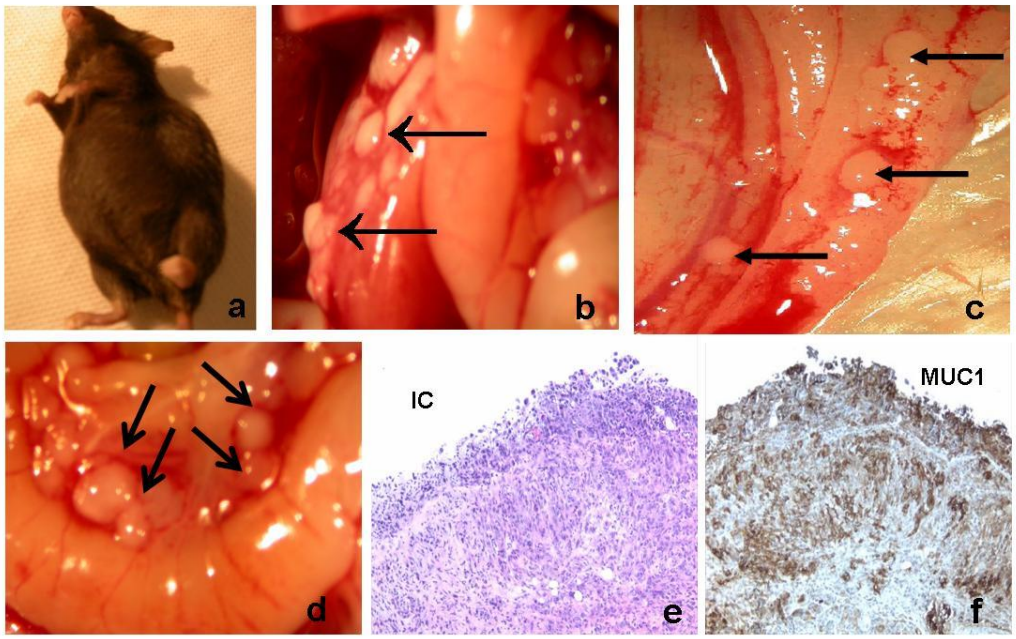

Fig. 4. Stable in vivo MUC1 expression in transplantable IG10-MUC1 syngeneic tumors. Five MUC1 mice were subjected to intraperitoneal (IP) injection of 5 x 106 IG10-MUC1 syngeneic cells. The injected cells induced tumor formation, accompanied by the accumulation of ascites (a). Representative pictures from one of the injected mice are shown. The tumors were spread throughout the peritoneal cavity and were often seen in the liver (b) peritoneum (c) and mesenteric (d), as pointed by arrows. Tumors were harvested and analyzed for MUC1 expression by IHC (e, f). Negative staining with an isotype control (IC) antibody is shown in (e). MUC1 presence appears as brown staining (f).

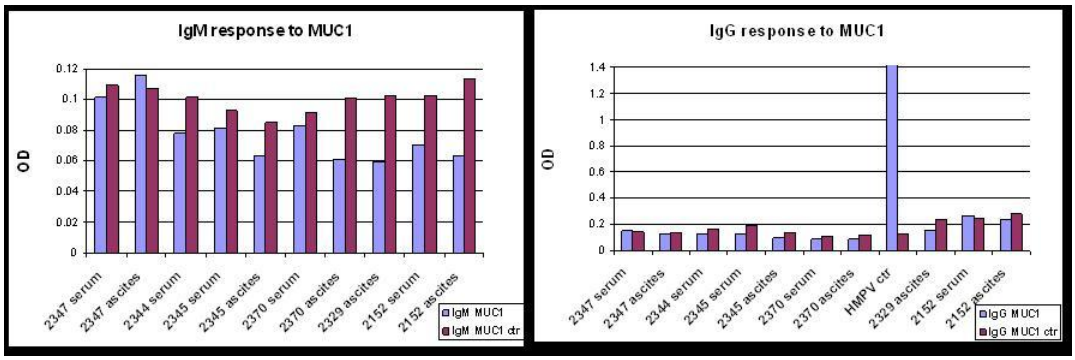

Fig. 5. No antibodies to MUC1 of IgM (right) or IgG isotype could be detected in serum and/or ascites of double Tg mice, despite some mice (2344, 2370) having high levels of circulating MUC1 (Table 1). The blue bars represent OD readings from experimental (MUC1-coated wells); burgundy bars represent OD from control (bovine serum albumin, BSA) coated wells. No significant increases were detected in any of the experimental wells over the control wells. The only above-control readings came from the IgG control antibody (HMPV).